BLOCK COPOLYMER BASED TARGETED NANOCARRIERS FOR NEUROENDOCRINE CANCER

by
Damla Demirkol
B.S. Chemistry, Boğaziçi University, 2021

Submitted to the Institute for Graduate Studies in
Science and Engineering in partial fulfillment
of the requirements for the degree of
Master of Science

Graduate Program in Chemistry
Boğaziçi University
2023

Dedicated to Linda McMillan

ACKNOWLEDGEMENTS

I would like to first of all express my deepest gratitude to Prof. Rana Sanyal for her invaluable mentorship. Her guidance throughout my studies has been irreplaceable on both an academic and personal level, and I deeply appreciate her encouragements, patience, support and insightful feedbacks. I continue to be inspired by her achievements in the field of nanomedicine and as an entrepreneur.

I would like to extend my gratitude to Prof. Amitav Sanyal for his extensive support and contributions to my studies, feedbacks and suggestions for my project and for inspiring me to immerse myself in organic synthesis as an undergraduate student.

I am grateful to Asst. Prof. Özgül Gök Özata for accepting to be in my defense jury and for their time, careful and constructive review of the final manuscript, and valuable comments.

I wish to sincerely thank Tuğçe Ataş for her endless support, patience, mentorship and guidance throughout my research and laboratory work, which was crucial for the success of this project, as well as her friendship.

I want to extend my thanks to Damla Kayhan and Dr. Aysun Değirmenci for their contribution in my project by performing the *in vitro* cell experiments.

I would like to thank my lab mates Enfal Çivril, Dr. Aysun Değirmenci, Goncagül Filiz, Sena Erbaş, Ece Günalan İnci and Dr. İsmail Altınbaşak for their friendship, guidance and support throughout my laboratory work.

I wish to express my heartfelt thanks to Linda McMillan, my dear friend and a remarkable neuroendocrine cancer survivor, for her courage and resilience which has been a constant source of inspiration. I am profoundly grateful for her unwavering support, which has shaped my journey.

Finally, I would like to express my sincere thanks and gratitude to my family for believing in me, and for their endless love and support.

I would like to thank The Scientific and Technological Research Council of Türkiye (TÜBİTAK) for financial support as part of the 2210-A graduate scholarship program. Funding by the Health Institutes of Türkiye (TÜSEB) (Project No. 4073) and Boğaziçi University Research Fund (BAP-ADP No. 50008) is gratefully acknowledged.

ABSTRACT

BLOCK COPOLYMER BASED TARGETED NANOCARRIERS FOR NEUROENDOCRINE CANCER

Neuroendocrine tumors pose significant challenges in terms of effective treatment due to their heterogeneous nature and limited therapeutic options. The focus of this study is to address these challenges through the development of targeted polymeric micelles for the codelivery of 5-fluorouracil (5-FU) and ribociclib, a CDK4/6 inhibitor, to neuroendocrine tumors. This novel approach involves the synthesis of a 5-FU monomer, two types of amphiphilic block copolymers, and subsequent functionalization of one of the block copolymers with a targeting peptide. In this study, a polymerizable 5-FU monomer was prepared, and two types of block copolymers were synthesized using reversible addition-fragmentation chain transfer (RAFT) polymerization. One type of block copolymer was non-targeted, while the other contained an NHS group, and was functionalized with cRGDfK peptide via activated ester-amine chemistry, providing targeting capability. Micelles loaded with ribociclib were prepared using the synthesized block copolymers, and their size, stability, and drug loading were characterized. *In vitro* release studies of 5-FU and ribociclib from the micelles were conducted in buffer solutions. Cytotoxicity assays were performed on two neuroendocrine tumor cell lines using targeted and non-targeted ribociclib-loaded micelles, as well as non-targeted micelles. Additionally, the internalization of non-targeted and targeted micelles in these cells was evaluated. The results demonstrate the successful synthesis of a targeted polymeric micellar nanocarrier capable of delivering both 5-FU and ribociclib to neuroendocrine tumors. All micelles showed cytotoxic effect on the cell lines, and targeted micelles were internalized faster compared to the non-targeted micelles, indicating their potential for improved tumor-specific delivery of multiple therapeutic agents to effectively combat these challenging tumors.

ÖZET

NÖROENDOKRİN KANSER İÇİN BLOK KOPOLİMER BAZLI HEDEFLİ NANOTAŞIYICILAR

Nöroendokrin tümörler, heterojen yapıları ve sınırlı tedavi seçenekleri nedeniyle etkili tedavi açısından önemli zorluklar oluşturmaktadır. Bu çalışmanın odak noktası, 5-fluorourasil (5-FU) ve ribosiklib'in nöroendokrin tümörlere ulaştırılması için bir hedefli polimerik misel nanotaşıyıcı sistemin geliştirilmesi yoluyla, bu zorlukları ele almaktır. Bu yeni yaklaşım, bir 5-FU monomerinin ve amfifilik blok kopolimerlerin sentezini ve ardından bir hedefleme peptidi ile kopolimerlerin işlevselleştirmesini içerir. Amfifilik blok kopolimerleri oluşturmak için, polimerize edilebilir bir 5-FU monomeri hazırlandı ve iki tür blok kopolimer, tersinir ekleme parçalanma zincir transferi (RAFT) polimerizasyonu kullanılarak sentezlendi. Bir blok kopolimer hedeflenmemişken, diğeri NHS grubu içeriyordu ve bu kopolimer aktifleştirilmiş ester-amin kimyası aracılığıyla cRGDfK peptidi ile fonksiyonelleştirilerek hedefleme yeteneği sağlandı. Sentezlenen blok kopolimerler kullanılarak ribosiklib yüklü miseller hazırlandı ve boyutları, stabiliteleri ve ilaç yüklemeleri karakterize edildi. 5-FU ve ribosiklib'in misellerden *in vitro* salım çalışmaları, tampon çözeltilerde gerçekleştirildi. Hedefli ve hedeflenmemiş ribosiklib yüklü misellerin yanı sıra hedeflenmemiş miseller kullanılarak, iki nöroendokrin tümör hücre hattı üzerinde sitotoksisite deneyleri yapıldı. Ek olarak, hedefli ve hedeflenmemiş misellerin bu hücrelerde içselleştirilmesi değerlendirildi. Sonuçlar, nöroendokrin tümörlere hem 5-FU hem de ribosiklib sağlayabilen hedeflenmiş bir polimerik misel nanotaşıyıcının başarılı sentezini göstermektedir. Hücrelerde tüm miseller sitotoksik etki gösterdi ve hedefli miseller hedeflenmemiş misellere kıyasla daha hızlı içselleştirildi. Bu sonuçlar, hedefli misellerin bu zorlu tümörlerle etkili bir şekilde mücadele etmek için çoklu terapötik ajanların gelişmiş tümöre özgü iletimi için potansiyelini işaret ediyor.

TABLE OF CONTENTS

LIST OF FIGURES

LIST OF TABLES

LIST OF ACRONYMS/ABBREVIATIONS

ACN	Acetonitrile
AIBN	2,2′-Azobis(2-methylpropionitrile)
ATRP	Atom Transfer Radical Polymerization
CCK-8	Cell Counting Kit-8
$CDCl_3$	Deuterated Chloroform
CDK 4/6	Cyclin Dependent Kinases 4/6
CI	Combination Index
CMC	Critical Micelle Concentration
cRGDfK	Cyclo (Arg-Gly-Asp-D-Phe-Lys)
cRGDfV	Cyclo (Arg-Gly-Asp-D-Phe-Val)
CTA	Chain Transfer Agent
CPADB	4-Cyano-4-(phenylcarbonothioylthio)pentanoic acid
DAPI	4′,6-diamidino-2-phenylindole
DLS	Dynamic Light Scattering
DCM	Dichloromethane
DMAC	N,N-Dimethylacetamide
DMAP	4-Dimethylaminopyridine
DMF	Dimethyl formamide
DMSO	Dimethyl sulfoxide
EC_{50}	Half Maximal Effective Concentration
EPR	Enhanced Permeation and Retention
FDA	Food and Drug Administration
GPC	Gel Permeation Chromatography
HPLC	High-Performance Liquid Chromatography
J	Coupling constant
kDa	Kilo Dalton
LC-MS	Liquid Chromatography-Mass Spectrometry
MeOH	Methanol
MHz	Mega Hertz
Mn	Number average molecular weight

NET	Neuroendocrine Tumor
NHS	N-Hydroxy Succinimide
NMP	Nitroxide-Mediated Polymerization
NMR	Nuclear Magnetic Resonance
NP	Nanoparticle
NR	Nile Red
OEGMEMA	Oligo (ethylene glycol) methyl ether methacrylate
PBS	Phosphate Buffer Solution
PDI	Polydispersity Index
PEG	Poly (ethylene glycol)
PTFE	Polytetrafluoroethylene
RAFT	Reversible Addition-Fragmentation Chain Transfer
RDRP	Reversible Deactivation Radical Polymerization
ROP	Ring Opening Polymerization
SCPDB	4-Cyano-4-(phenylcarbonothioylthio)pentanoic acid *N*-succinimidyl ester
TEA	Triethylamine
THF	Tetrahydrofuran
5-FU	5-fluorouracil

1. INTRODUCTION

1.1. Cancer

Cancer is characterized by the uncontrolled proliferation and metastasis of abnormal or damaged cells in the body. It can originate from virtually any location within the human body which consists of trillions of cells. Normally, cells undergo mitotic division to produce new cells that fulfill physiological needs, whereas old or injured cells are eliminated through apoptosis, and are replaced by fresh ones (Figure 1.1). However, this precise mechanism occasionally becomes dysfunctional, allowing abnormal or compromised cells to proliferate in an uncontrolled manner (Figure 1.2). Consequently, these cells can aggregate and form masses of tissues known as tumors. Tumors can be either benign or malignant (cancerous). Benign tumors remain confined to their local regions and do not spread to distant organs or tissues. Cancerous tumors, on the other hand, can invade neighboring tissues and eventually spread to remote parts of the body, leading to the formation of new cancerous tissue, a phenomenon referred to as metastasis [1].

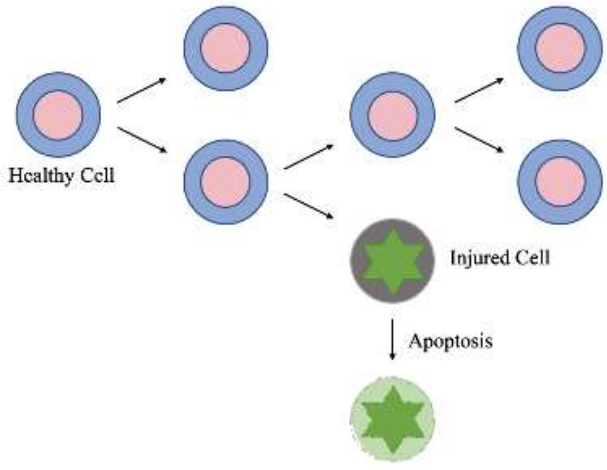

Figure 1.1. Normal cell division.

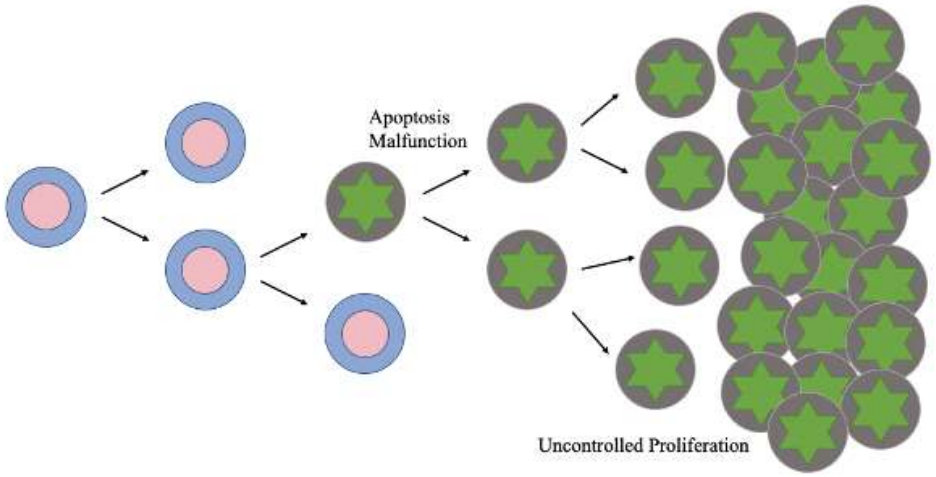

Figure 1.2. Cancer cell division.

According to the World Health Organization (WHO), cancer remains the second most prevalent cause of death worldwide in the 21st century after cardiovascular disease, accounting for nearly 10 million deaths in 2020 (Figure 1.3). Age-standardized world rates indicate that the incidence rate of cancer is approximately 220 in 100,000 for men and 185 in 100,000 for women, with a combined mortality rate of approximately 90 cancer deaths per 100,000 people. Global Cancer Observatory (GLOBOCAN) estimates an increase in the annual incidence of cancer from 19 million cases in 2020 to approximately 30 million cases in 2040 as well as an increase in the number of deaths caused by cancer annually from 10 million cancer deaths in 2020 to around 16 million in 2040 [2, 3].

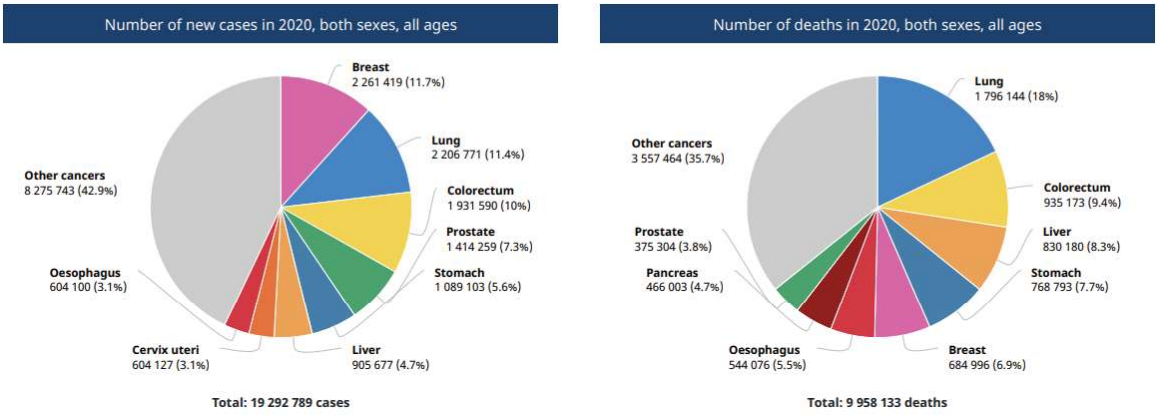

Figure 1.3. Reported new cancer cases and deaths worldwide in 2020 [2].

1.2. Nanocarriers for Cancer Treatment

Conventional treatments for cancer are mainly chemotherapy, radiation therapy and surgery, while in some cases hormonal therapy, immunotherapy and targeted therapy can be utilized. Surgical removal of tumors is most effective in the early stages of cancer, when it is possible to remove all cancer cells. However, in many cases, surgery is not an option due to metastases in other sites in the body, or is only performed to reduce tumor size and improve quality of life. When surgery is not an option, chemotherapy and radiation therapy are used, often in combination. These treatments can cause cell death in a fraction of cancerous cells, but they cannot fully eliminate all of them [4].

Chemotherapy involves the use of cytotoxic anticancer drugs to kill metabolically active cells in the body, as cancer cells are known to generally divide and multiply at a faster rate than most healthy cells. Although it is an indispensable cancer treatment method, it has several limitations. The biggest drawback of conventional chemotherapy is that it is a systemic therapy, meaning that the cytotoxic agents are distributed nonspecifically in the body where they affect healthy cells as well as cancer cells, causing severe side effects related to systemic toxicity, such as the suppression of the immune system, making the patient more susceptible to other, possibly infectious diseases. Another downside of cancer treatment by chemotherapy is that prolonged exposure of cancer cells to chemotherapy is known to cause drug resistance, called multidrug resistance syndrome (MDRS), and can limit the therapeutic efficacy of the treatment significantly [4, 5].

Due to the prevalence and high mortality rates of cancer despite current treatment options, researchers have been developing novel drug carriers called drug delivery systems such as polymeric nanoparticles, polymeric micelles, liposomes and dendrimers (Figure 1.4) over the past decades, in order to deliver the cytotoxic drug in a targeted manner to the tumor tissue. These nanocarriers aim to provide a controlled and sustained release of the cytotoxic drug at the tumor site, thereby significantly decreasing the side effects of chemotherapy, while providing a high dose of the drug to the cancer cells, overcoming the nonspecific biodistribution and targeting, low bioavailability, low water solubility, low protein binding, and systemic toxicity of chemotherapeutic agents [6, 7].

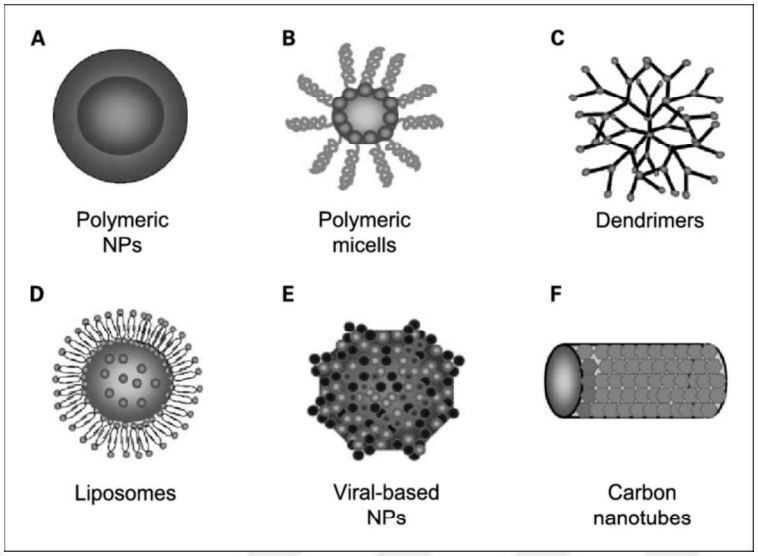

Figure 1.4. Drug delivery systems for cancer therapy. Reprinted from reference [5] with permission from AACR.

The Food and Drug Administration (FDA) has approved several drug delivery systems to improve cancer treatment, including those based on polymeric micelles, liposomes, and polymeric nanoparticles. One notable example is Genexol-PM®, a polymeric micelle formulation containing paclitaxel approved by the FDA in 2016 (Figure 1.5). These polymeric micelles, composed of biocompatible and biodegradable materials, help improve the solubility and stability of paclitaxel, allowing for enhanced drug delivery and increased efficacy in treating various cancers, such as breast, lung, and ovarian cancer [8].

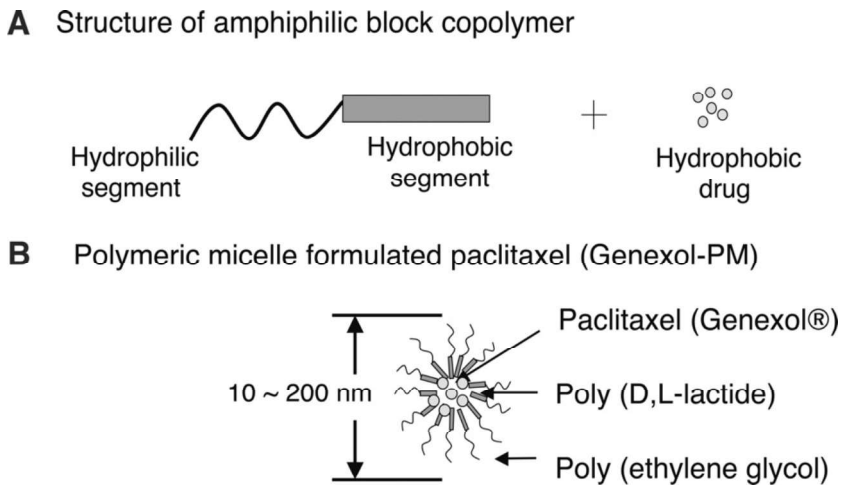

Figure 1.5. Formulation of polymeric micelles Genexol-PM® [8].

Onivyde®, also known as PEP02, is a liposomal nanoparticle used for the delivery of irinotecan. These liposomes, composed of phospholipids, encapsulate irinotecan and improve its pharmacokinetics and biodistribution. Onivyde® was approved by the FDA in 2015 for the treatment of metastatic pancreatic cancer and has shown improved efficacy compared to conventional irinotecan formulations [9]. Abraxane®, a drug delivery system that utilizes albumin-bound nanoparticles for paclitaxel delivery, was also approved by the FDA in 2005. These nanoparticles provide improved solubility and targeted drug delivery, leading to enhanced pharmacokinetics and therapeutic outcomes in various cancers, including breast, lung, and pancreatic cancer [10].

These and other FDA-approved drug delivery systems demonstrate the significant progress in utilizing polymeric nanoparticles, dendrons, albumin binding formulations and liposomes to enhance the delivery of anticancer drugs, improve therapeutic efficacy, and minimize side effects for better patient outcomes. In recent research, specifically polymer based nanoparticles (NPs) as nanocarriers of antineoplastic drugs have shown significant potential in improving cancer therapeutics as well. For instance, in the treatment of brain tumors, Çırpanlı et al. used camptothecin-loaded cyclodextrin NPs in a rat glioma model. Through local delivery of the nanoparticle suspension via injection, the nanomaterials protected the drug from hydrolysis, leading to improved survival times [11]. Similarly, Guo et al. developed paclitaxel-containing PEG–PLGA NPs coated with a DNA aptamer that binds to a protein that is highly expressed in glioma cells. This formulation demonstrated higher tumor growth inhibition compared to conventional paclitaxel-NPs, indicating its potential for targeted therapy [12].

Polymeric NPs have also been widely investigated for use in the treatment of breast cancer. Yuan et al. loaded curcumin and doxorubicin in pH-sensitive NPs and the NPs showed promising results in terms of improving cell uptake, retention, and cytotoxicity, offering a potential strategy for overcoming drug resistance [13]. Additionally, Hu et al. developed oxygen-generating theranostic NPs comprising poly(ε-caprolactone-co-lactide)-b-PEG-b-poly(ε-caprolactone-co-lactide), doxorubicin, chlorin e6, and colloidal MnO_2. These NPs generated oxygen in the tumor environment, alleviating tumor hypoxia and enhancing the efficacy of photodynamic therapy and doxorubicin treatment [14].

Liver cancer, one of the leading causes of cancer-related mortality, has also witnessed advancements in polymeric nanoparticle-based therapies. Zhu et al. synthesized nanoparticles based on galactosamine-conjugated polydopamine-modified copolymers and tested it *in vitro* and *in vivo* against HepG2 cells, targeting them via asialoglycoprotein receptor-mediated recognition. Docetaxel-loaded NPs exhibited superior inhibition of cell proliferation and reduced tumor size compared to conventional formulations, demonstrating the potential of polymeric NPs in liver cancer treatment [15].

The safer, less toxic, and more tumor-specific treatment provided by these polymeric nanocarriers is possible due to passive and, in some cases, active targeting. These two phenomena, especially passive targeting, give large molecular weight nanocarriers cancer cell targeting abilities and make it possible to introduce high doses of cytotoxic drugs to the tumor, while protecting noncancerous and otherwise healthy tissue from the cytotoxic effect of the drug. Therefore, passive and active targeting should be considered when designing novel drug carriers.

1.2.1. Passive Targeting (EPR Effect)

Passive targeting, also known as enhanced permeability and retention (EPR) effect, was first described in 1986 by Maeda and Matsumura, who observed that macromolecules with a molecular weight greater than 40 kDa could accumulate in tumors through leaky blood vessels [16]. Since then, the concept of the EPR effect has been widely studied and utilized in the field of nanomedicine.

The EPR effect is a phenomenon that explains the accumulation nanoparticles, liposomes or other such macromolecules in tumor tissue due to the increased permeability and decreased lymphatic drainage of tumor vasculature. This effect is one of the main strategies for targeted drug delivery to cancer cells, as it allows for selective accumulation of therapeutic agents in tumor tissues while protecting healthy cells [17]. The mechanism behind the EPR effect involves the unusual structure of blood vessels in tumors. Tumor vessels are known to be irregularly shaped, tortuous, and dilated, with a high density of pores and wide gaps between endothelial cells. This allows for increased permeability of

macromolecules into tumor tissue, as well as decreased lymphatic drainage due to the lack of functional lymphatic vessels in tumors [18]. EPR effect is illustrated in Figure 1.6.

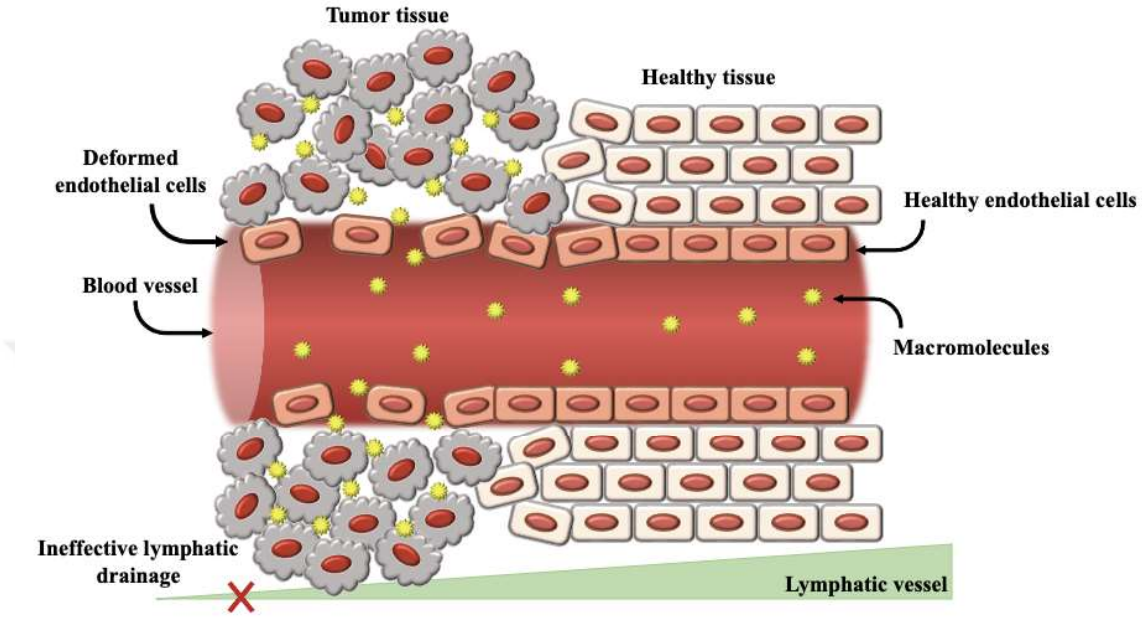

Figure 1.6. The EPR effect.

An important factor in the EPR effect is the size of the macromolecules. Generally, macromolecules with a size range of 10-200 nm accumulate the most in tumors, as they can easily penetrate the leaky vasculature while avoiding rapid clearance. Additionally, the surface properties of nanoparticles or liposomes can affect their accumulation in tumors. For example, particles with a positive charge may interact more strongly with negatively charged tumor cells, leading to increased accumulation [19].

The EPR effect has been successfully utilized in the development of nanomedicines for cancer treatment. For example, liposomal formulations of doxorubicin and paclitaxel have been approved for clinical use due to their ability to accumulate in tumor tissues via the EPR effect. Other types of nanoparticles, such as gold nanoparticles and dendrimers, have also been investigated for their potential use in targeted drug delivery [20].

Despite its promising potential, the EPR effect has some limitations. One of the main challenges is the heterogeneity of tumor vasculature, which can affect the degree and location of macromolecule accumulation. Additionally, the EPR effect is not specific to tumors, and increased accumulation may be seen in some normal tissues with larger gaps between endothelial cells, such as the liver and spleen [21].

Overall, the EPR effect is a powerful strategy for targeted drug delivery to tumors, allowing for selective accumulation of therapeutic agents in tumor tissues while sparing healthy cells. The abnormality in tumor vasculature, namely, increased permeability and decreased lymphatic drainage, plays a key role in this phenomenon.

1.2.2. Active Targeting

Active targeting of tumors is a promising approach to improve the effectiveness of cancer treatments. By using targeted nanoparticles, drugs or imaging agents can be selectively accumulated in tumor tissues. The principle behind active tumor targeting is to exploit the unique characteristics of cancer cells, such as overexpressed receptors, to deliver therapeutic agents specifically to the tumor site as illustrated in Figure 1.7 [22]. This approach is especially useful in poorly vascularized tumors, since EPR effect in these tissues is limited [23]. Designing nanoparticles with specific targeting abilities that can overcome physiological barriers is the key to utilizing active tumor targeting.

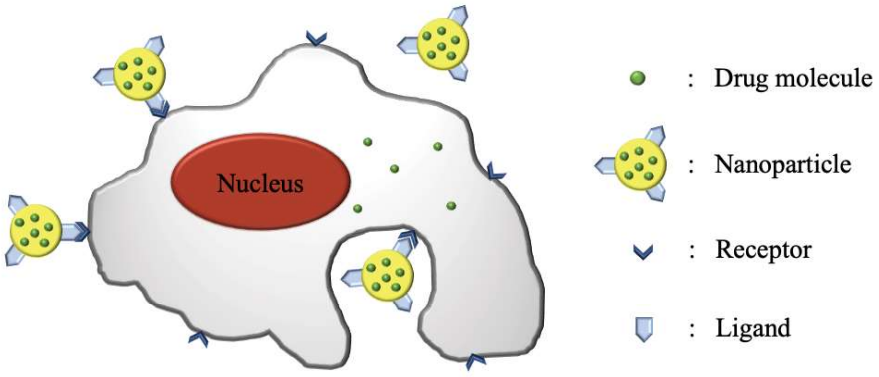

Figure 1.7. Active targeting.

In recent years, advances in nanotechnology have led to the development of various strategies for active tumor targeting, including surface modification with targeting ligands, stimuli-responsive materials, and microenvironment-responsive nanoparticles. Often, a combination of these approaches is incorporated into drug delivery systems to further enhance the effectiveness of delivery.

Surface modification with targeting ligands is widely used to achieve active tumor targeting. The most commonly used ligands are antibodies, peptides and aptamers that can specifically bind to tumor-specific biomarkers [24]. For example, Liu et al. developed nanoparticles conjugated with a cyclic peptide that targets the $\alpha_v\beta_3$ integrin, which is overexpressed on the surface of various cancer cells [25]. The nanoparticles were loaded with a platinum drug, and showed enhanced anticancer activity and internalization in glioblastoma cells *in vitro* and *in vivo* [26]. Similarly, Cheng et al. developed targeted silica nanoparticles by conjugating a folate ligand to the surface of the nanoparticle. Folate receptor is another receptor that is overexpressed on the surface of many kinds of cancer cells [27], and the doxorubicin nanoparticles showed enhanced tumor accumulation and tumor growth inhibition in folate receptor-positive tumor models [28].

Stimuli-responsive materials have also been developed for active tumor targeting. These materials include various polymers that can respond to specific external stimuli (exogenous) or stimuli in the tumor microenvironment (endogenous), such as low pH, high temperature, or enzyme activity, enabling the controlled release of drugs at the tumor tissue [30] (Figure 1.8). For example, Cui et al. developed doxorubicin loaded nanoparticles self-assembled from a pH-sensitive prodrug, transferrin-poly(ethylene glycol)-curcumin. The nanoparticles showed enhanced tumor accumulation and antitumor activity in a mouse model of breast cancer [31]. Long et al. synthesized mesoporous silica nanoparticles grafted with a temperature-responsive polymer, polycaprolactone, for the controlled release of doxorubicin. The nanoparticles remained structurally stable in physiological conditions, showed fast and complete release of doxorubicin at high temperatures, and induced apoptosis in different cancer cell lines [32].

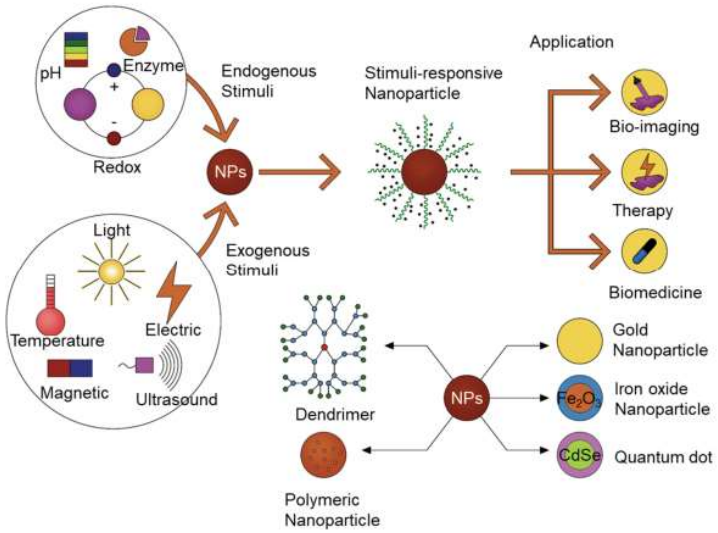

Figure 1.8. Stimuli-responsive nanoparticles for bioimaging, therapy and biomedicine applications [29].

Nanoparticles that can respond to the unique features exhibited in the tumor microenvironment, such as hypoxic and acidic conditions, and selectively deliver drugs to the cancer cells have shown promise as nanocarriers as well [33]. Many acid-responsive drug delivery systems have recently been designed based on the acidity of tumor tissues [34–39]. As an example, Wei et al. designed an enzyme- and pH-sensitive branched copolymer-doxorubicin conjugate that forms nanoparticles which exhibit pH-sensitive drug release, show enhanced accumulation in breast tumors, and demonstrate apoptosis of breast tumor cells without causing obvious systemic toxicities [37]. Zhai et al., on the other hand, designed redox responsive core cross-linked micelles using PEG-b-PBSe diblock copolymers for dual drug delivery, which showed increased drug release in the presence of glutathione *in vitro*, and enhanced tumor growth suppression *in vivo* [39].

Active tumor targeting is overall a promising approach for improving the specificity and efficacy of anticancer therapies. The strategies developed for active tumor targeting, including surface modification with targeting ligands, stimuli-responsive materials, and microenvironment-responsive nanoparticles have shown very promising results with respect to nontargeted therapies in preclinical studies and hold great potential for future clinical applications. Design of drug delivery systems using active targeting strategies should be occupied to maximize the efficiency of cancer treatment.

1.3. Polymeric Micelles as Nanocarriers

Polymeric micelles were first used as nanocarriers of anti-cancer molecules by Bader et al. in 1984, where in vitro studies showed sustained drug release from the construct [40]. Since then, there has been extensive effort in developing polymeric micelles for the treatment of cancer, due to their ability to address the poor solubility, low bioavailability, systemic toxicity and poor pharmacokinetics of many anti-cancer drugs. Polymeric micelles generally have sizes between 10-100 nm and are therefore facile drug carriers due to EPR effect [19].

Polymeric micelles are mainly self-assembled nanoparticles obtained from amphiphilic or multifunctional block copolymers at concentrations higher than the critical micelle concentration (CMC). These polymers possess end-to-end hydrophobic and hydrophilic chains, which gives the structure the ability to both attract and repel water in aqueous environments, resulting in the formation of the hydrophilic corona and hydrophobic core of polymeric micelles. Polymeric micelles are able to successfully encapsulate hydrophobic drug moieties in their core due to hydrophobic interactions [22]. Self-assembly of block copolymers can take place in several routes depending on the structure of the block copolymer. The micelle formation process for a diblock copolymer above its CMC is shown in Figure 1.9 to illustrate the general self-assembly process of block copolymers into micelles.

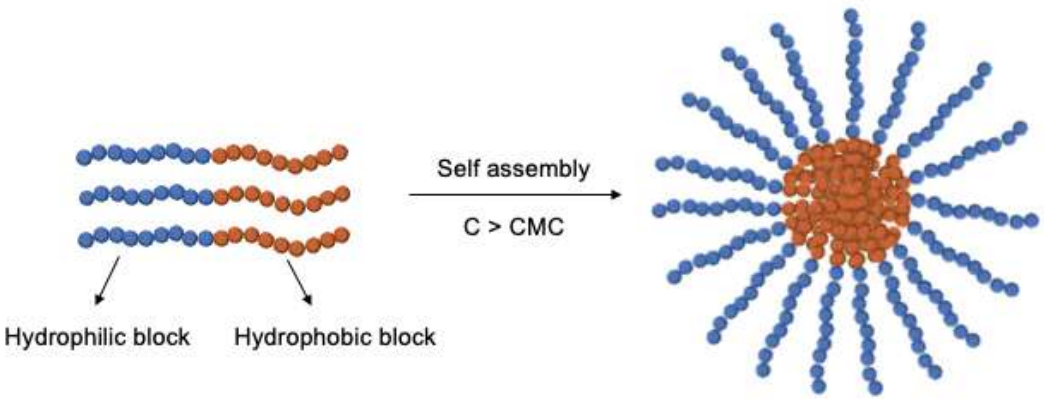

Figure 1.9. Formation of polymeric micelles from diblock copolymers in aqueous media above CMC.

Polymeric micelles using diblock or triblock copolymers are prepared via a variety of methods such as direct dissolution, solvent evaporation and dialysis. Solvent evaporation, or cosolvent evaporation, is used when the polymer and drug are insoluble in water. In this method, the polymer and drug are mixed in water miscible volatile solvents, and water is added dropwise to form emulsions. Upon the evaporation of volatile solvents, the solution contains polymeric micelles suspended in water [41].

The degree of interactions between drug molecules and the micellar core is critical for the drug loading, encapsulation efficiency, micellar stability and drug release kinetics of polymeric micelles [42]. Hydrophobic interactions and hydrogen-bonding interactions are usually the leading deterministic factors in these properties [43-45]. Thus, the design of novel polymeric micellar drug delivery systems should be approached considering these interactions, carefully and strategically determining the structure of each of the blocks on block copolymers..

The properties of polymeric micelles depend also on the properties of the polymers that are used as building blocks, such as their molecular weights, chemical structures and CMC values. Despite the diverse properties of polymeric micelles derived from different polymers, they generally demonstrate low CMC values in contrast to low molecular weight surfactants [46], making them stable upon dilution, and facilitating their circulation in blood without rapid dissociation. The dilution stability of micelles can be further enhanced through chemical modifications such as core cross-linking [47, 48].

Various types of polymers can be used for the hydrophilic corona of polymeric micelles, and polyethylene glycol (PEG) is widely utilized in research since it has been approved by the FDA for internal use [42]. Upon hydration, PEG forms polymer chains in the form of brushes, which stretch out from the micelle’s core, stabilizing the hydrophobic core and inter-micellar interactions via steric effects [49, 50]. In polymeric micelles with residual cationic charges in the core, PEG was proven to be crucial for preventing undesired interactions between negatively charged proteins in the plasma and the core of micelles, further stabilizing the construct [51].

The amphiphilic block copolymers can be tailored in order to achieve desired properties in the micellar nanoparticle. Modification of the end groups in hydrophilic corona with targeting units such as peptides, antibodies or aptamers can give the nanoparticle targeting abilities, whereas the hydrophobic core can be designed to incorporate more hydrophobic or less hydrophobic drugs, or imaging agents. Controlled release can be achieved by occupying stimuli-responsive polymer units in the corona [42].

1.3.1. RAFT Polymerization

As mentioned previously, the design of amphiphilic block copolymers is crucial for the final properties of polymeric micelles, so, different polymerization techniques are being utilized by researchers to obtain block copolymers with defined molecular weight and functionalization. Among the most commonly used and facile techniques are ring opening polymerization (ROP) and types of reversible deactivation radical polymerization (RDRP): nitroxide mediated polymerization (NMP), atom-transfer radical polymerization (ATRP), reversible addition-fragmentation chain transfer (RAFT) polymerization [52].

RDRP techniques have facilitated the synthesis of functional polymers with targeted molecular weights, narrow molecular weight distributions and defined architecture. The RDRP processes ATRP and NMP include a reversible activation-deactivation equilibrium between active and dormant states of the propagating polymer radicals through either nitroxide capping for NMP or via a redox process with a metal halide salt for ATRP, where the propagation takes place in the active state and the equilibrium is strongly favored towards the dormant state [53].

RAFT polymerization, although a type of RDRP, proceeds differently than others, through a degenerative chain transfer process, which significantly eliminates the formation of free radicals, and consequently, dead polymers. Because the mechanism does not include formation of radicals, an external radical source is required to initiate the reaction. The exact mechanism of RAFT is shown in Figure 1.10. The process begins with initiation, where radicals from the initiator are produced, and monomer units start to grow into short polymer chains. The thiocarbonylthio compounds (Z-C(=S)S-R), which are RAFT agents known as chain transfer agent (CTA), contribute in the next steps by binding to these short polymer

radical chains, and exchanging these polymer chains continuously in equilibrium so that all polymer chains have very similar number of monomer units. Through this reversible chain transfer, all polymer chains are given equal opportunity to grow, with a very small amount of dead polymers, significantly minimizing the PDI of the polymers obtained. When the polymerization is complete, most chains have the thiocarbonylthio end group, and the entire process can essentially be viewed as though the monomer units have been added between the S-R bond of the CTA [53].

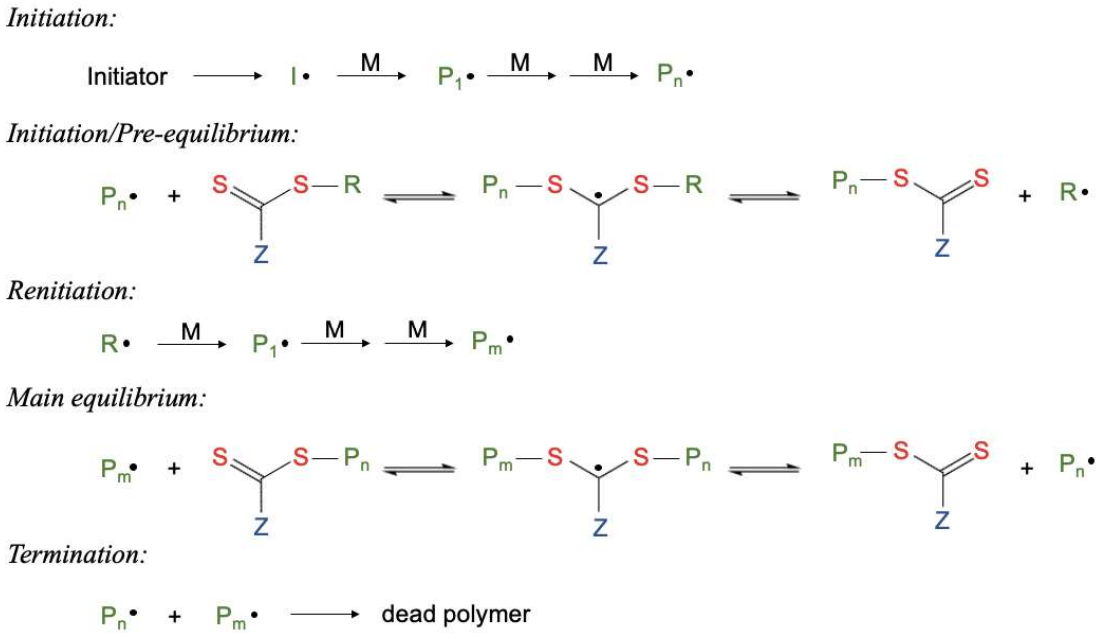

Figure 1.10. Mechanism of RAFT polymerization.

The choice of CTA is critical especially for block copolymer synthesis, since modifications to the Z and R end group functionalities of polymers such as attachment of targeting moieties or other polymer chains though click reactions may be desired [54, 55].

Of the RDRP techniques, RAFT polymerization has been widely used as a controlled living polymerization for drug delivery systems because of its compatibility with various monomers, control over the molar mass and polydispersity index (PDI) of obtained polymers and the lack of need for a metal catalyst [56].

1.4. Neuroendocrine Tumors (NETs) and Current Treatments

Neuroendocrine tumors (NETs), also called neuroendocrine neoplasms (NENs) or neuroendocrine carcinomas (NECs), are a unique group of tumors that arise from neuroendocrine cells that are present in various organs throughout the body, including the gastrointestinal tract, pancreas, lungs, and other locations rich in neuroendocrine cells [57]. These tumors are very similar to healthy neuroendocrine cells, which possess sacs filled with hormones and neurotransmitters to secrete upon demand (Figure 1.11) [58]. These secretions are irregulated in the case of NETs, and can lead to a range of clinical symptoms called carcinoid syndrome, depending on the specific tumor type. For instance, carcinoid tumors, a type of NET, often secrete serotonin, causing symptoms such as flushing and diarrhea [59, 60].

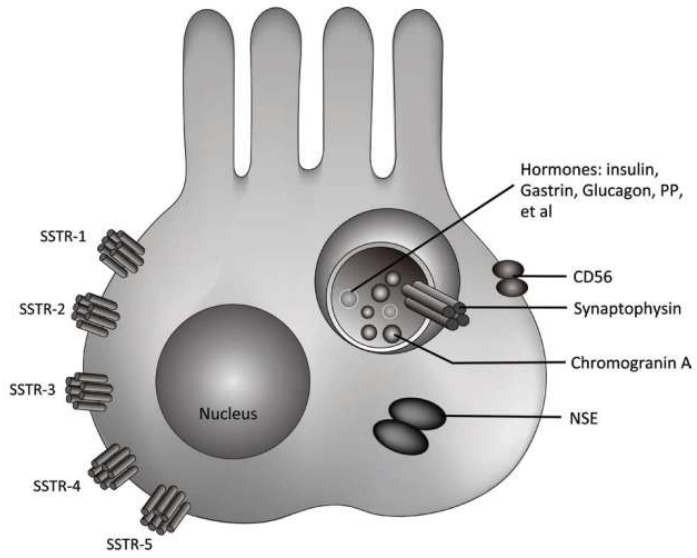

Figure 1.11. Schematical illustration of neuroendocrine cells and tumors [58].

Over the past few decades, there has been a noticeable increase in the incidence of NETs [61], as seen in Figure 1.12. This rise in cases has highlighted the need for further research into the underlying causes and optimal treatment approaches. The reasons for this increase depend on many factors, including improved diagnostic techniques, increased awareness, and a potential true rise in the occurrence of these tumors [62, 63].

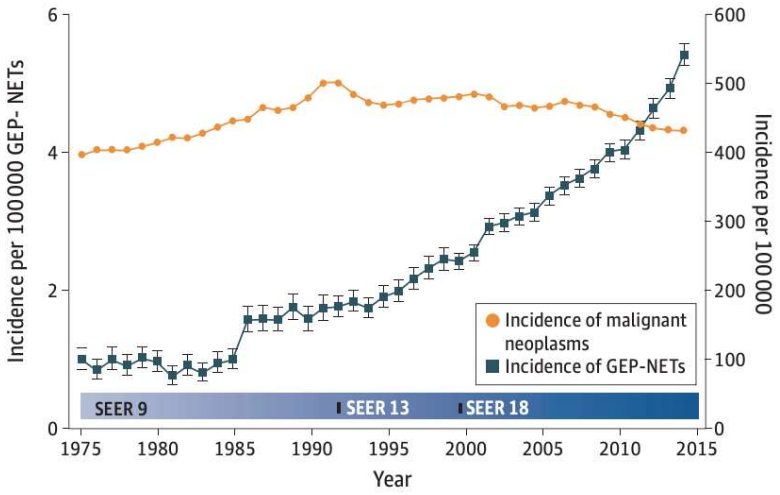

Figure 1.12. Incidence of gastroenteropancreatic neuroendocrine tumors in the United States over time [61].

Neuroendocrine tumors (NETs) present particular challenges in terms of treatment options due to their diverse nature and characteristics. As these tumors often arise from neuroendocrine cells in various organs, they have the potential to metastasize and spread beyond their initial site of origin. Although surgery is the only curative approach to NETs, this metastatic nature significantly impacts the feasibility of surgical intervention, making it risky or less viable in many cases [64].

Chemotherapeutic agents may be used, mostly in combination, for the management of NETs or as a preoperative systemic chemotherapy [65]. Ongoing clinical trials include regimens composed of combinations of 5-fluorouracil, streptozocin, doxorubicin, oxaliplatin, and everolimus [66–70]. Sadly, even combination chemotherapy often shows limited efficacy in NETs, due to the fact that these tumors often exhibit slow proliferation, and the anti-cancer agents that are used are most effective on fast growing cells [71]. Although some regimens such as FOLFOX (5-fluorouracil and oxaliplatin) [65] and CAPOX (capecitabine and oxaliplatin) [72] give better results, these tumors are generally more resistant to traditional chemotherapy agents compared to other types of tumors, resulting in poor response rates and limited overall benefits for patients [64–73]. As a result, the biological structure and properties of neuroendocrine cells as well as tumors are used to develop alternative approaches that focus on controlling tumor growth and relieving symptoms caused by the secretions.

Somatostatin analogues, such as octreotide and lanreotide, have emerged as a key treatment option for managing NETs [74]. The primary focus of such analogues is suppressing tumor activity and hormone secretion to ease symptoms by binding to somatostatin receptors that are usually overexpressed on NET cells [75]. In cases where surgical intervention is not feasible due to metastatic NETs, or after partial removal of tumors to improve quality of life, somatostatin analogues serve as a cornerstone of treatment.

While somatostatin analogues represent a significant advancement in the management of NETs, they mainly provide palliative benefits, and there remains a need for further research and exploration of alternative treatment options. As the efficacy of traditional chemotherapy is limited, novel therapeutic approaches and targeted interventions are being investigated. These approaches include peptide receptor radionuclide therapy (PRRT) [76], and the use of tyrosine kinase inhibitors (TKIs) [77], mammalian target of rapamycin (mTOR) inhibitors [78] and cyclin D-dependent kinases 4/6 (CDK4/6) inhibitors [79] to cause cell death in NETs.

1.4.1. Polymeric Micelles for NET Treatment

Researchers are actively exploring innovative drug delivery systems that can enhance the specificity and efficiency of treatments for NETs. These systems include the use of targeted nanoparticles, liposomes, and polymeric micelles, which can be functionalized with ligands or peptides to actively target the tumor cells. Such advancements hold the potential to revolutionize treatment outcomes by improving drug delivery, minimizing off-target effects, and maximizing the therapeutic efficacy for patients with NETs.

Most recently, Jaskula-Sztul et al. investigated the use of unimolecular micelles with dendrimeric cores for targeted neuroendocrine cancer therapy using the octreotide and KE108 peptides [80, 81]. The micelles that were conjugated with the KE108 peptide, a novel somatostatin analogue, exhibited excellent tumor-targeting abilities and demonstrated superior capabilities in suppressing neuroendocrine cancer cell growth *in vitro*, as well as high tumor accumulation and potent anticancer efficacy *in vivo* (Figure 1.13) [81].

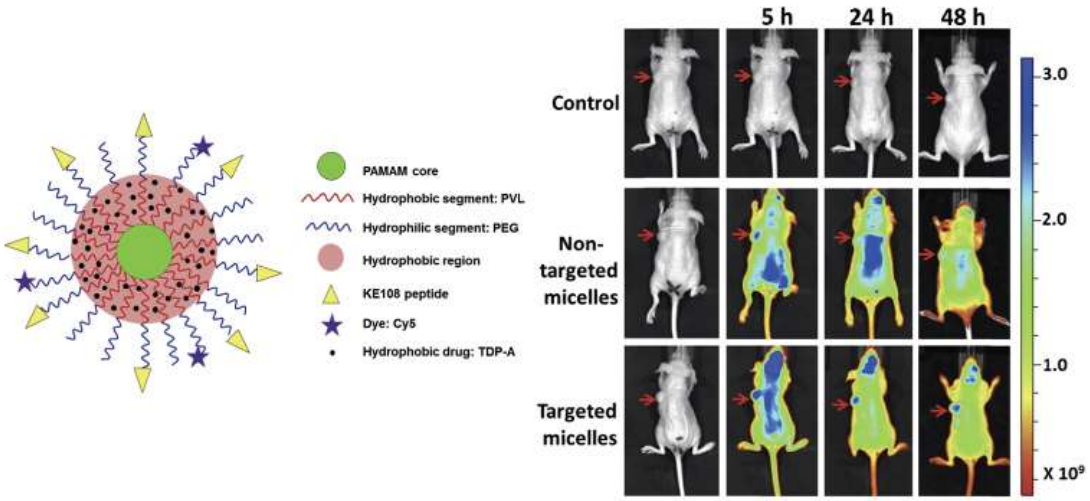

Figure 1.13. (a) Structure of KE108 conjugated unimolecular micelles and (b) *in vivo* fluorescence images of BON tumor bearing mice after treatment with KE108 conjugated unimolecular micelles. (Reprinted from reference [81] with permission from Elsevier.)

Other drug delivery systems for NETs that are being investigated by researchers all around the world include gold nanoparticles [82, 83], antibody-drug conjugates [84, 85] and polymeric nanoparticles [86]. Application of nanoparticles as imaging agents for NETs is also a widely researched topic [87], owing to the difficulty of diagnosis of NETs. Due to the increasing incidence of neuroendocrine type carcinomas and the variety of these types of cancers, such innovative approaches to the delivery of therapeutic or imaging agents carry immense importance in the struggle against NETs.

2. AIM OF THE STUDY

The aim of this study is to develop polymeric micellar nanoparticles using 5-FU conjugated and cRGDfK peptide functionalized amphiphilic block copolymers loaded with ribociclib, a CDK4/6 inhibitor, for the targeted treatment of neuroendocrine tumors. Neuroendocrine tumors represent a significant medical challenge due to their limited treatment options and resistance to conventional therapies. Polymeric micellar nanoparticles have emerged as promising drug delivery systems for various types of cancers, offering enhanced drug stability, controlled release, and targeted delivery to tumor sites. However, the synthesis and efficacy of these nanoparticles for neuroendocrine tumor treatment remain underexplored. This study aims to explore the successful synthesis of cRGDfK functionalized and 5-FU bearing amphiphilic block copolymers and their self-assembly into stable ribociclib loaded polymeric micellar nanoparticles, as well as the *in vitro* drug release profiles from these micelles. Furthermore, the study aims to determine the therapeutic efficacy of the ribociclib loaded micelles against neuroendocrine tumor cell lines compared to free drug administration by cytotoxicity experiments, and provide insights into the effectiveness of the targeting strategy of NETs via the cRGDfK peptide by comparing the cellular uptake of targeted and non-targeted micelles in these cell lines.

3. EXPERIMENTAL

3.1. Materials

Acetonitrile (ACN), triethylamine (TEA), tetrahydrofuran (THF), dichloromethane (DCM), dimethylformamide (DMF), methanol (MeOH), acetone, formaldehyde and all other solvents were HPLC grade, purchased from Merck and used without further purification. Methacrylic anhydride, oligo(ethylene glycol) methyl ether methacrylate (OEGMEMA, Mn= 300g/mol), 4-Cyano-4-(phenylcarbonothioylthio)pentanoic acid (CPADB), 4-Cyano-4-(phenylcarbonothioylthio)pentanoic acid *N*-succinimidyl ester (SCPDB), 2,2'-azobis(2-methylpropionitrile) (AIBN), pyrene, 4-dimethylaminopyridine (DMAP) were purchased from Sigma-Aldrich. 5-Fluorouracil was purchased from TCI Chemicals.

3.2. Instrumentation

Preparatory HPLC with a Shim-pack PREP-ODS column (length/ID 20 x 250 mm, 15 μm particle size) was used for the purification of drug monomer. Monomer and polymers were characterized using ^{1}H-NMR spectroscopy (Varian 400 MHz). Molecular weight and polydispersity index (PDI) values of polymers were analyzed using gel permeation chromatography (GPC) with a Shimadzu PSS-SDV column (length/ID 8 x 300 mm, 10 μm particle size), 0.05 M lithium bromide in DMAC as the eluent and a flow rate of 1.0 mL/min. Micelles were characterized with dynamic light scattering (DLS) using a Malvern Zetasizer Nano ZS photometer, and fluorescence spectroscopy using a Cary Eclipse Fluorescence Spectrophotometer. Concentrations of 5-FU and Ribociclib in solutions in drug release or drug loading studies were also measured using LC-MS (Shimadzu, Japan). LC-MS was further used to determine the purity of monomer before polymerization.

3.3. Synthesis of Polymerizable 5-FU Monomer (5FUMA)

The synthesis of polymerizable 5-FU monomer was performed in two steps according to literature protocol [88]. First, 5-FU (1 g, 7.68 mmol) and formaldehyde (37 wt.%, aq., 512 mg, 17.05 mmol) were stirred under N_2 in a 50 mL round bottom flask at 60 °C for 6 h. The resulting oily crude was lyophilized for 2 days. For the second step, lyophilized crude was dissolved in 12 mL anhydrous ACN. TEA (1.24 g, 12.29 mmol) was then added to the solution. Methacrylic anhydride (1.18 g, 7.68 mmol) was added to the reaction solution dropwise at 0 °C in 5 min. Reaction continued at 0 °C for 1 h, then at room temperature for 16 h. After reaction was completed, ACN was evaporated via rotary evaporator. Crude was dissolved in 50 mL DCM and extracted with saturated $NaHCO_3$ (25 mL x 2) and distilled water (50 mL x 1). DCM phases were combined and dried over anhydrous Na_2SO_4, and solvent was evaporated. The 5FUMA monomer was purified by preparatory HPLC with ultrapure water and ACN as mobile phases (1:1, v/v). After evaporating ACN via rotary evaporator, the monomer was extracted from water with DCM (5 x 50 mL). Organic phase was dried over anhydrous Na_2SO_4 and DCM was evaporated using rotary evaporator and product was dried under reduced pressure to give 507 mg of 5FUMA as solid white crystals (29.0 % yield). ^{1}H NMR ($CDCl_3$, δ, ppm): 7.69 (d, J= 5.4 Hz, 1H); 6.25 (s, 1H); 5.73 (d, J= 7.1 Hz, 2H); 1.96 (s, 1H).

3.4. Synthesis of p(OEGMEMA) and NHS-p(OEGMEMA)

Reversible addition-fragmentation chain transfer (RAFT) polymerization was used for the synthesis of homopolymers p(OEGMEMA) and NHS activated p(OEGMEMA). For the synthesis of p(OEGMEMA) polymer, OEGMEMA (1.0 g, 3.33 mmol) and CPADB (55.8 mg, 0.20 mmol) were dissolved in 7 mL DMF. To the reaction mixture, AIBN (5.47 mg, 0.033 mmol) dissolved in 100 μL DMF was added. The reaction mixture was purged with N_2, then polymerization was allowed to take place for 20 h in an oil bath at 70 °C. Polymerization was stopped by removing the mixture from the heat source and exposing it to air. DMF was evaporated using a rotary evaporator, and the polymer was purified by precipitation in cold diethyl ether thrice. After drying under reduced pressure, a viscous polymer precipitate containing approximately 21 OEGMEMA repeating units was obtained. (820 mg, 82 % yield).

For the synthesis of NHS- p(OEGMEMA), SCPDB (63 mg, 0.167 mmol) was used as the chain transfer agent and the procedure was followed with the same amounts for OEGMEMA and AIBN to obtain a viscous polymer precipitate with approximately 24 OEGMEMA repeating units. (995 mg, 93 % yield).

3.5. Synthesis of p(OEGMEMA)-b-p(5FUMA) and NHS-p(OEGMEMA)-b-p(5FUMA) Block Copolymers

For the synthesis of block copolymers p(OEGMEMA)-*b*-p(5FUMA) and NHS-p(OEGMEMA)-*b*-p(5FUMA), p(OEGMEMA) and NHS-p(OEGMEMA) were used as macro chain transfer agents respectively. To synthesize p(OEGMEMA)-*b*-p(5FUMA), p(OEGMEMA) (500 mg, 0.0769 mmol) and 5FUMA (713 mg, 3.127 mmol) were dissolved in DMF (2.50 mL). To the reaction mixture, AIBN (1.71 mg, 0.0104 mmol) dissolved in 100 µL DMF was added. The reaction mixture was purged with N_2, and polymerization was allowed to take place for 24 h in an oil bath at 70 °C. Polymerization was stopped by removing the mixture from the heat source and exposing it to air. DMF was evaporated using a rotary evaporator, and the polymer was purified by precipitation in diethyl ether thrice. After drying under reduced pressure, solid polymer precipitate with approximately 38 5FUMA repeating units was obtained. (900 mg, 74 % yield). For the synthesis of NHS-p(OEGMEMA)-*b*-p(5FUMA), NHS-p(OEGMEMA) (100 mg, 0.0133 mmol) was used as macro chain transfer agent and the same procedure was followed with 5FUMA (114 mg, 0.499 mmol) and AIBN (0. mg, 0.00166 mmol) to obtain solid polymer precipitate with approximately 32 5FUMA repeating units. (165 mg, 78 % yield).

3.6. Synthesis of cRGDfK- p(OEGMEMA)-*b*-p(5FUMA) Block Copolymer

Activated ester-amine reaction was utilized for the attachment of the cRGDfK peptide to the block copolymer NHS-p(OEGMEMA)-*b*-p(5FUMA). For this reaction, cRGDfK (3.40 mg, 0.00563 mmol), NHS-p(OEGMEMA)-*b*-p(5FUMA) (76.3 mg, 0.00512 mmol) and DMAP (0.628 mg, 0.00512 mmol) were dissolved in 460 µL DMF and solution was stirred at room temperature for 20 hours. The product was purified by dialysis using a dialysis membrane with a 3.5 kDa molecular weight cut-off against a mixture of MeOH and H_2O (4:1, v/v) to remove unreacted cRGDfK, DMAP and the NHS leaving group. After

evaporation of the solvent and drying under reduced pressure, cRGDfK- p(OEGMEMA)-*b*-p(5FUMA) was obtained. (57 mg, 71 % yield).

3.7. Critical Micelle Concentration (CMC) Measurements

Solutions containing block copolymer with concentrations ranging from 4 x 10^{-9} M to 4 x 10^{-5} M and 6 x 10^{-7} M pyrene in 3 mL water were prepared by solvent evaporation technique for CMC measurements. For this, first, stock solutions of pyrene and the block copolymer were prepared in acetone. Constant volume (10 μL) of the pyrene stock solution and varying volumes of the block copolymer stock solutions were transferred into 15 vials and final acetone volume was made 700 μL for each vial. 3 mL distilled water was then added dropwise to each solution while shaking gently. The organic solvent was evaporated in a well ventilated hood overnight. Fluorescence spectroscopy measurements were carried out for all samples. Pyrene excitation spectra between 300 and 360 nm were recorded at emission wavelength 390 nm for each sample and CMC values were calculated using the ratio between the fluorescence intensities at 338 nm and 334 nm as a function of the logarithm of polymer concentration.

3.8. Formation of Non-Targeted and Targeted Polymeric Micelles

In order to obtain ribociclib loaded non-targeted polymeric micellar nanoparticles, p(OEGMEMA)-*b*-p(5FUMA) (3 mg, 0.000204 mmol) and ribociclib (0.16 mg, 0.000363 mmol) were mixed in acetone in a 10 mL round bottom flask. To this solution, 3 mL distilled water was added dropwise, and acetone was evaporated using rotary evaporator at 37 °C and 85 rpm, so that micellar nanoparticles were obtained by cosolvent evaporation technique. The obtained micelle solution was centrifuged at 13000 rpm for 10 minutes and filtered with a PTFE 0.45μm filter.

For the formation for targeted ribociclib loaded polymeric micellar nanoparticles, a mixture of cRGDfK-p(OEGMEMA)-*b*-p(5FUMA) and p(OEGMEMA)-*b*-p(5FUMA) (1/4, w/w), and ribociclib were used. Rest of the procedure was the same as the preparation of ribociclib loaded non-targeted micellar nanoparticles. To form targeted or non-targeted micellar nanoparticles without ribociclib, the procedures were followed with polymers only.

DLS measurements for all micelle solutions were performed to obtain the size and PDI of micellar nanoparticles. Drug loading of ribociclib loaded micelles was determined by mixing 100 μL of micelle solution with 400 μL ACN and analyzing these samples in LC-MS using a calibration curve for ribociclib between 5 – 100 ppm.

3.9. Stability of Polymeric Micelles

To determine the stability of ribociclib loaded micelles upon serial dilution with water, first, a ribociclib loaded micelle solution with 1 x 10^{-5} M block copolymer concentration was prepared, and DLS measurements were taken. The solution was then diluted two fold by pipetting 500 μL of it and mixing with 500 μL water. After taking the DLS measurements of the diluted micelle solution, the dilution and DLS measurement process was repeated up to a dilution factor of 1024. DLS measurements were used to determine the percent of nanoparticles in the solution by volume, and the average sizes of diluted micelles.

For lyophilization stability, micelles were prepared by cosolvent evaporation as described before, and drug loading and DLS measurements were performed. 1 mL of micelle solution was freeze-dried using lyophilizer, then dissolved in 1mL water to reconstitute micelles. DLS measurements of lyophilized sample was taken and micelles were filtered with a PTFE 0.45μm filter before drug loading measurements.

3.10. *In vitro* Drug Release from Polymeric Micelles

To perform the *in vitro* drug release studies, non-targeted micelle solutions containing p(OEGMEMA)-*b*-p(5FUMA) (9.5 mg, 0.000625 mmol) and ribociclib (0.5 mg, 0.00115 mmol) in each 1 mL of solution were prepared via cosolvent evaporation as mentioned earlier. The micelle solution was taken in a dialysis bag prepared from a dialysis membrane with a 3.5 kDa molecular weight cut-off, and the bag was dipped in 10 mL PBS (pH 7.4), Acetate Buffer (pH 5.5) or Carbonate Buffer (pH 10.5) solutions. 100 μL of the buffer was removed at sampling times and the drug concentrations in the samples were analyzed in LC-MS using a calibration curve for ribociclib between 5 mg/L – 100 mg/L and a calibration curve for 5-FU between 0.5 mg/L – 50 mg/L.

3.11. *In vitro* Cytotoxicity of Polymeric Micelles on Neuroendocrine Tumor Cells

CCK-8 assay was performed to determine the cytotoxicity of micelles and free drugs on two cell lines, NCI-H727 human pulmonary carcinoid tumor cells and BE(2)-C neuroblastoma cell line. 5000 BE(2)-C cells per well in DMEM/F12 media (100μL) and 15000 NCI-H727 cells per well in RPMI media (%1 Penicillin-Streptomycin) (100μL) were seeded on a 96-well plate, and incubated for 24 hours. Stock solutions of micelles and free drugs were prepared to contain 1 x 10^{-3} M of drug, and these solutions were diluted 10-fold to obtain series of solutions with concentrations ranging from 1 x 10^{-4} M to 1 x 10^{-13} M. Cell media were replaced with 100 μL solutions of different concentrations of 5-FU, ribociclib, ribociclib loaded non-targeted micelles, empty non-targeted micelles and ribociclib loaded targeted micelles in triplicates, and cells were incubated at 37 °C, BE(2)-C cells for 48 hours and NCI-H727 cells for 72 hours. The toxicity of free drugs and micelles was examined using CCK-8 cell viability assay. After incubation time was up, free drug or micelle solutions in the wells were discarded, and 10 μL of the CCK-8 solution and 90 μL of fresh medium was added to each well. Cells were incubated for 1–4 hours, and absorbance values at 450 nm were measured using a microplate reader after incubation to determine the percent of viable cells. EC_{50} values were calculated by GraphPad prism software using non-linear regression mode.

3.12. Internalization of Polymeric Micelles in Neuroendocrine Tumor Cells

Nile red loaded non-targeted and targeted micelles were prepared by solvent evaporation technique to visualize the internalization of micelles in NCI-H727 and BE(2)-C cells. Nile red (0.9 mg, 0.00283 mmol) and p(OEGMEMA)-*b*-p(5FUMA) (3.00 mg, 0.000197 mmol) in 3 mL H_2O for Nile red loaded non-targeted micelles. Same amount of Nile red, and a mixture of p(OEGMEMA)-*b*-p(5FUMA) (2.40 mg, 0.000158 mmol) and cRGDfK-p(OEGMEMA)-*b*-p(5FUMA) (0.6 mg, 0.0000390 mmol) in 3 mL H_2O was used for Nile red loaded targeted micelles. NCI-H727 and BE(2)-C cells (100000 cells/well) were separately seeded in 12-well plates as duplicates in 1 mL of RPMI and DMEM/F12 media, respectively. The cells were incubated at 37 °C for 24 h. Micelle solutions were diluted 10 times with corresponding cell media, and Nile red loaded non-targeted micelle solution, Nile red loaded targeted micelle solution, and free Nile red with the same concentration of Nile

red (0.03 mg/mL) were added to the wells. In addition to these, the cells were incubated with both the Nile red loaded targeted micelle solution and free cRGDfV peptide as a competitive ligand. After 1h and 3h incubation, solutions were removed and cells were washed with 1 x PBS (1 mL x 2 times). Cells were fixed by using 3.7% formaldehyde solution at 37 °C for 10 min. After the fixation process, cells were washed with 1 x PBS (1 mL x 2 times). Then, cell nuclei were stained with DAPI for 15 min at 37 °C. After washing the cells, cell images were taken using a Zeiss Observer Z1 fluorescence microscope at room temperature and processed with Zeiss Zen Blue lite software.

4. RESULTS AND DISCUSSION

The first part of synthesis was the synthesis of the 5-FU bearing monomer since it is a building block for the targeted and non-targeted block copolymers. After monomer synthesis, homopolymers and block copolymers were synthesized, and the synthesis scheme for the homopolymers and block copolymers is illustrated in Figure 4.1.

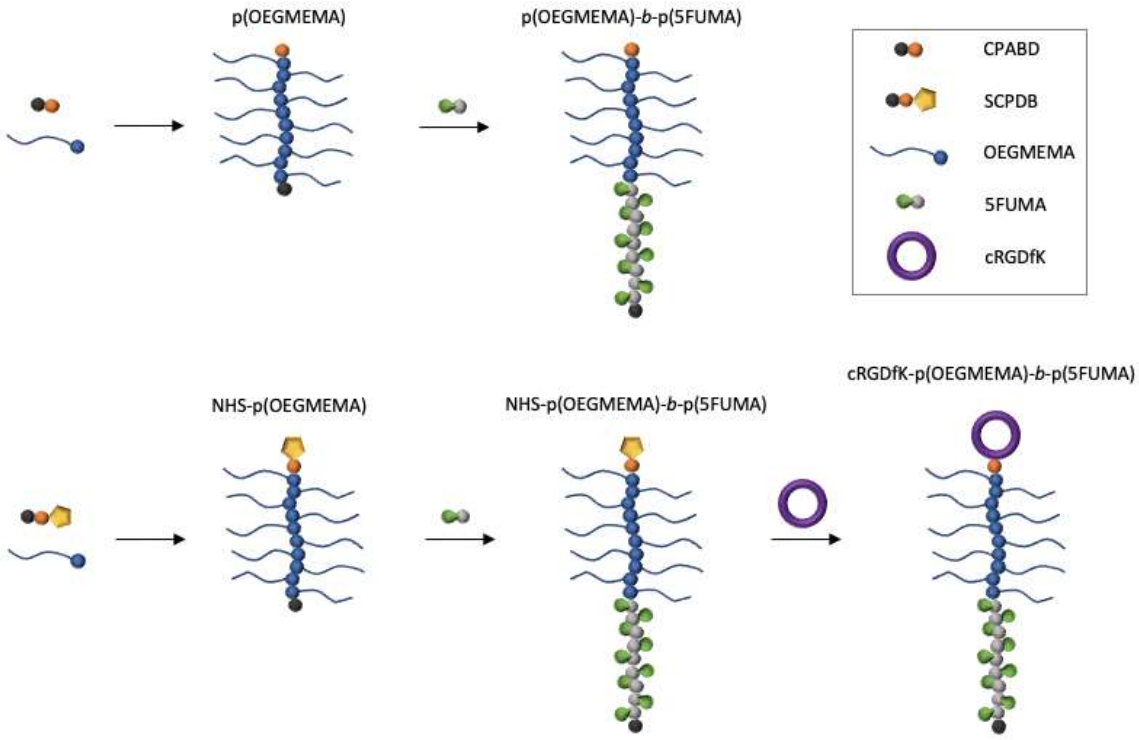

Figure 4.1. Overall synthesis scheme of non-targeted and targeted block copolymers.

4.1. Synthesis and Characterization of Polymerizable 5-FU Monomer (5FUMA)

The 5-FU monomer, 5FUMA, was synthesized according to literature protocol in two steps [88]. First, 5-FU was reacted with formaldehyde to obtain 5FU-OH. (Figure 4.2)

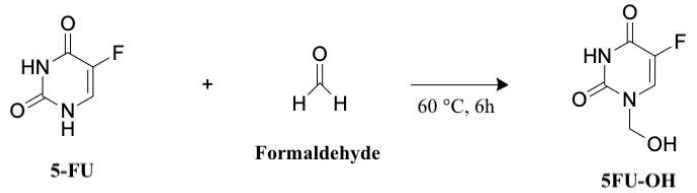

Figure 4.2. First step of the synthesis of 5FUMA.

For the second step, 5FU-OH was reacted with methacrylic anhydride in order to attach a double bond to the drug molecule via an ester bond. (Figure 4.3) Characterization of 5FUMA monomer was done by ^{1}H-NMR. (Figure 4.4)

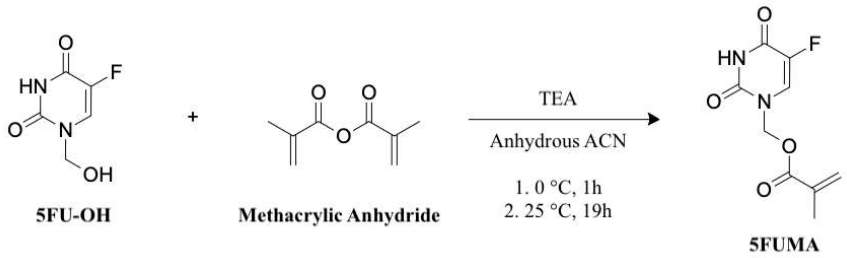

Figure 4.3. Second step of the synthesis of 5FUMA.

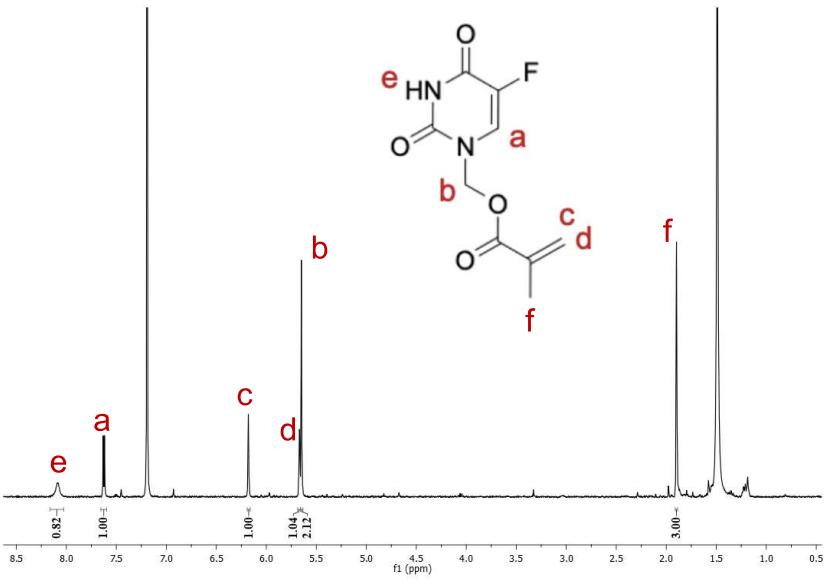

Figure 4.4. ^{1}H-NMR spectrum of 5FUMA.

4.2. Synthesis and Characterization of p(OEGMEMA) and NHS-p(OEGMEMA)

RAFT polymerization was occupied to synthesize the macro chain transfer agents p(OEGMEMA) and NHS-p(OEGMEMA) (Figure 4.5 and Figure 4.6). For the synthesis of NHS-p(OEGMEMA), same conditions as p(OEGMEMA) were used while using SCPDB instead of CPADB as chain transfer agent in order to introduce an NHS group that can later be used for peptide attachment.

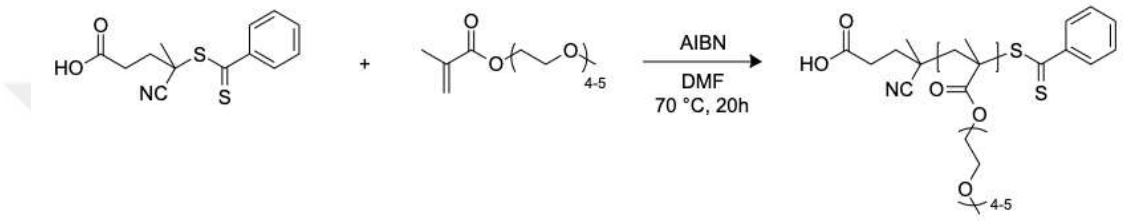

Figure 4.5. Synthesis of p(OEGMEMA).

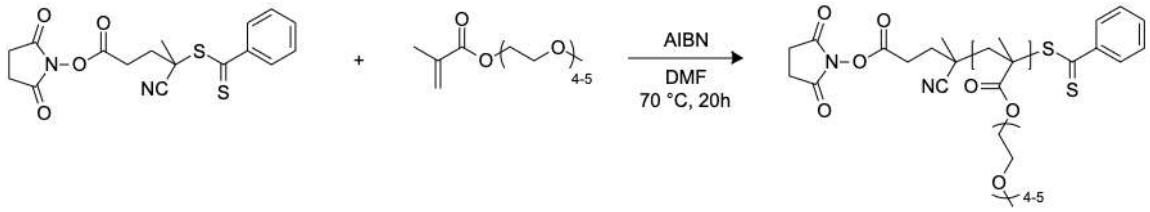

Figure 4.6. Synthesis of NHS-p(OEGMEMA).

Polymers with similar molecular weights and PDI values were obtained. The ^{1}H-NMR spectra of the polymers p(OEGMEMA) and NHS-p(OEGMEMA) indicated successful polymerization. This was determined due to the presence of proton resonances between 7.36-7.88 ppm of the aromatic protons of chain transfer agents, the proton resonances around 3.39 ppm due to the protons of the methyl ether terminal of OEGMEMA, and, in the case of NHS-p(OEGMEMA), the presence of proton resonances around 2.84 ppm indicating the succinimide protons (Figure 4.7 and Figure 4.8).

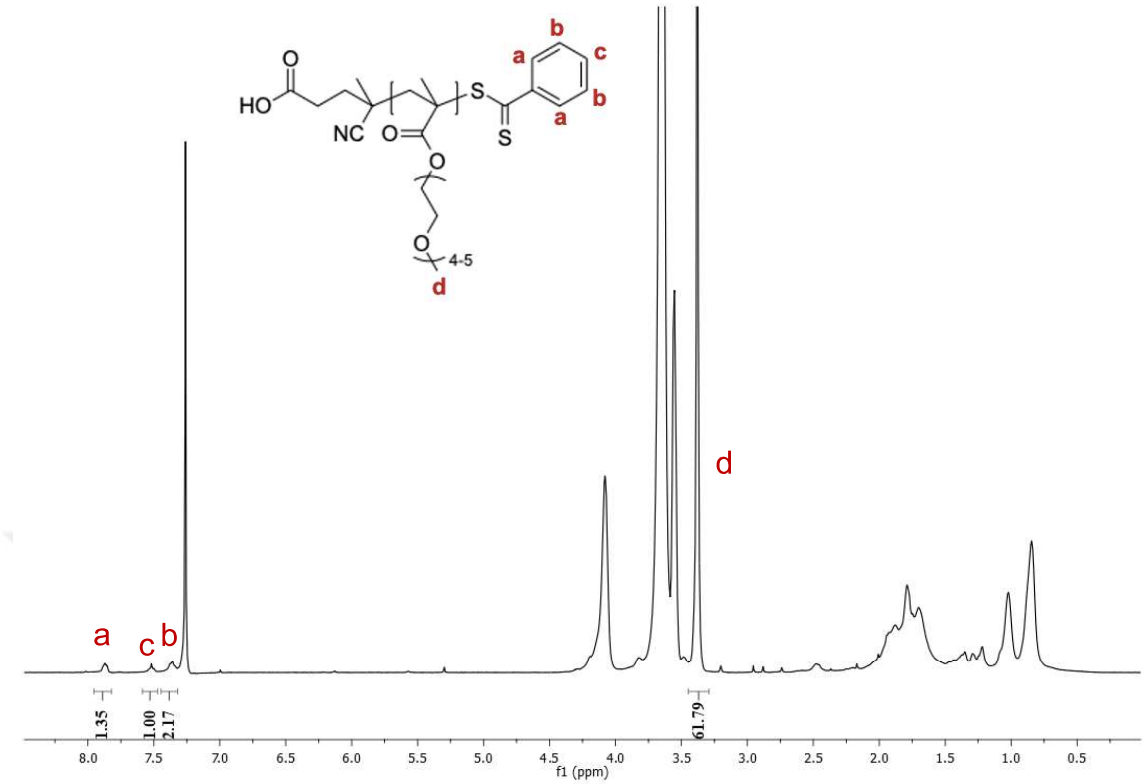

Figure 4.7. [1]H-NMR spectrum of p(OEGMEMA).

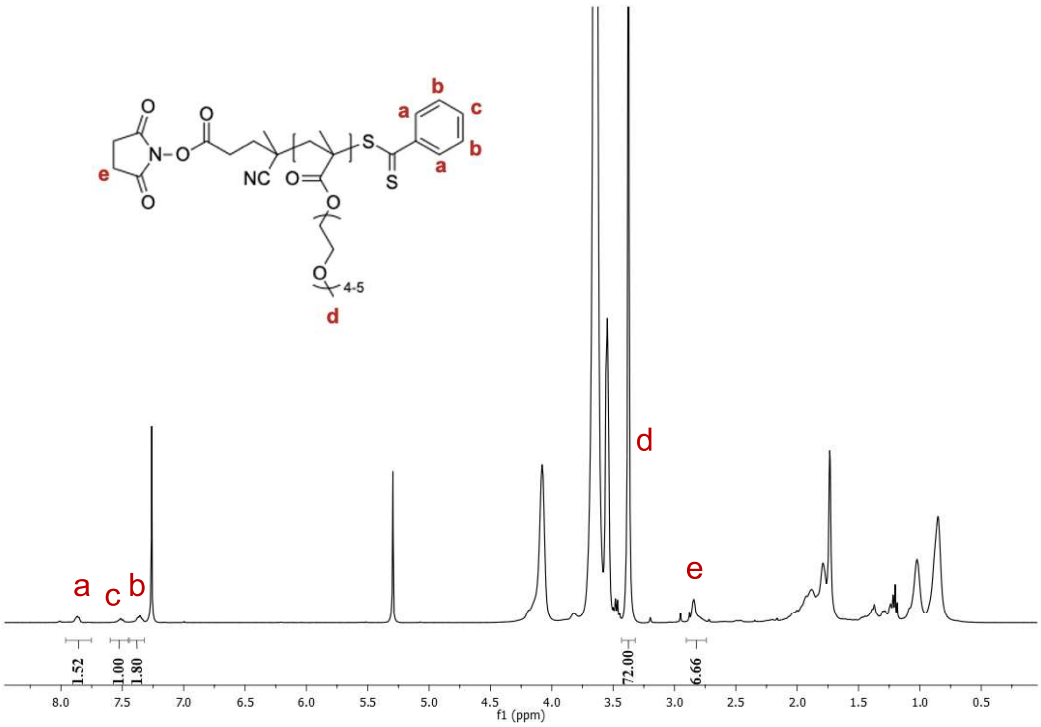

Figure 4.8. [1]H-NMR spectrum of NHS-p(OEGMEMA).

The number of OEGMEMA repeating units was calculated by comparing the integrations of proton resonances of aromatic protons of the chain transfer agent with the integrations of proton resonances of the terminal methyl ether protons of OEGMEMA. 21 OEGMEMA repeating units in p(OEGMEMA) and 24 OEGMEMA repeating units in NHS-p(OEGMEMA) were obtained. Molecular weight (Mn) and PDI values from GPC for p(OEGMEMA) and NHS-p(OEGMEMA) were found to be 5.83 kDa, 1.186 and 6.05 kDa, 1.210, respectively.

4.3. Synthesis and Characterization of p(OEGMEMA)-*b*-p(5FUMA) and NHS-p(OEGMEMA)-*b*-p(5FUMA) Block Copolymers

For the synthesis of non-targeted and NHS functionalized block copolymers p(OEGMEMA)-*b*-p(5FUMA) and NHS-p(OEGMEMA)-*b*-p(5FUMA) by RAFT polymerization, p(OEGMEMA) and NHS-p(OEGMEMA) homopolymers were used as macro chain transfer agents respectively, and 5FUMA was used as the building block for polymerization (Figure 4.9 and Figure 4.10). The conditions of polymerization were same for both block copolymers.

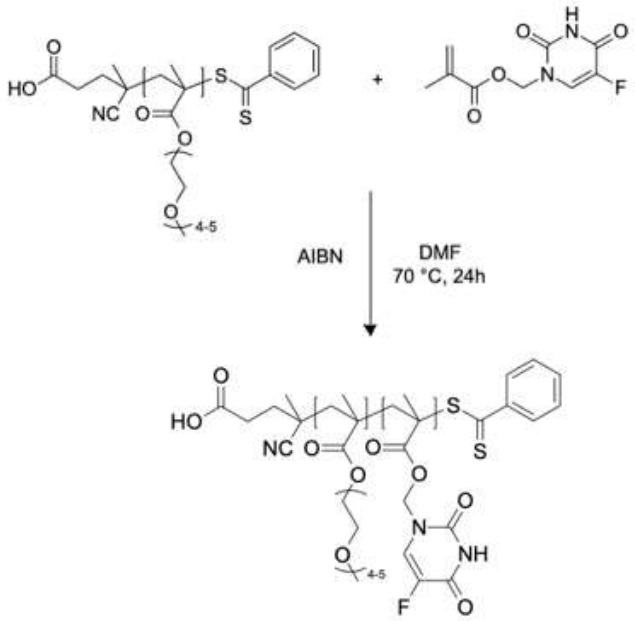

Figure 4.9. Synthesis of p(OEGMEMA)-*b*-p(5FUMA).

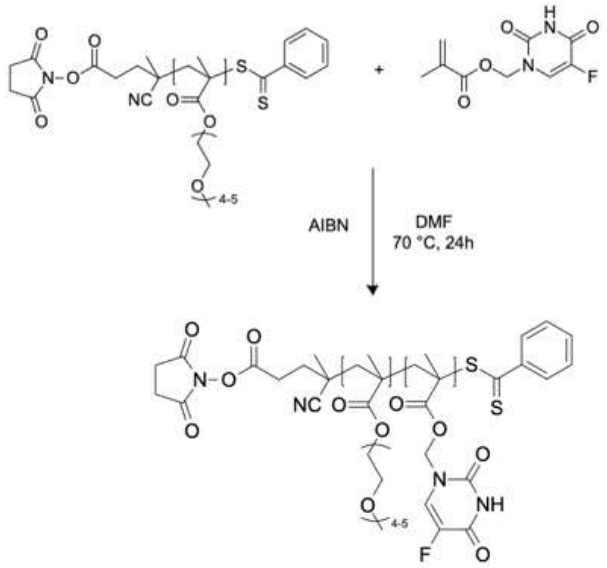

Figure 4.10. Synthesis of NHS-p(OEGMEMA)-*b*-p(5FUMA).

In the ^{1}H-NMR spectra of p(OEGMEMA)-*b*-p(5FUMA) and NHS-p(OEGMEMA)-*b*-p(5FUMA) in DMSO, the presence of the proton resonances around 8.11 ppm and 5.5 ppm due to protons of the 5FUMA unit proved successful polymerization (Figure 4.11 and Figure 4.12).

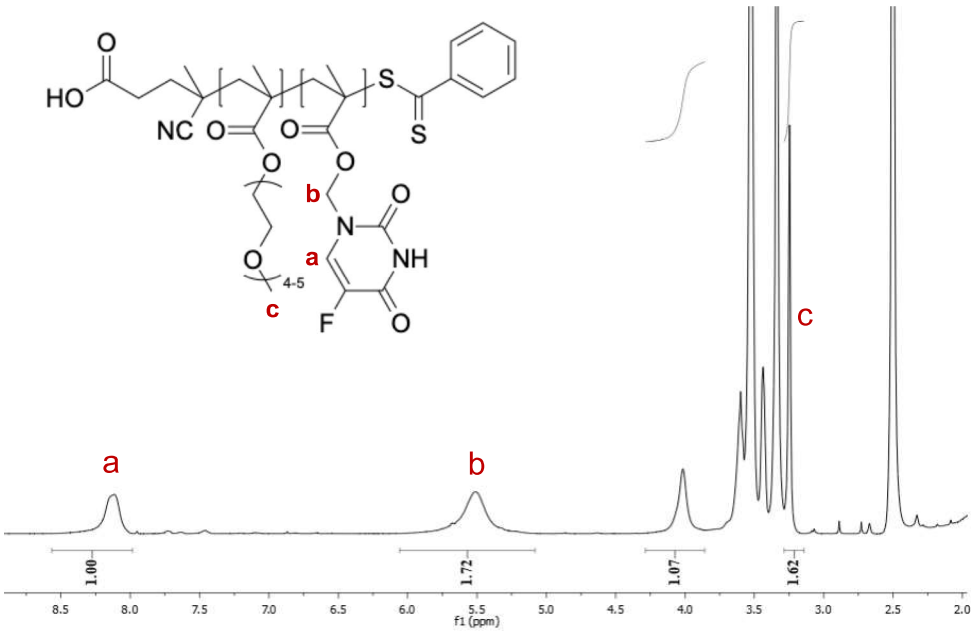

Figure 4.11. ^{1}H-NMR spectrum of p(OEGMEMA)-*b*-p(5FUMA).

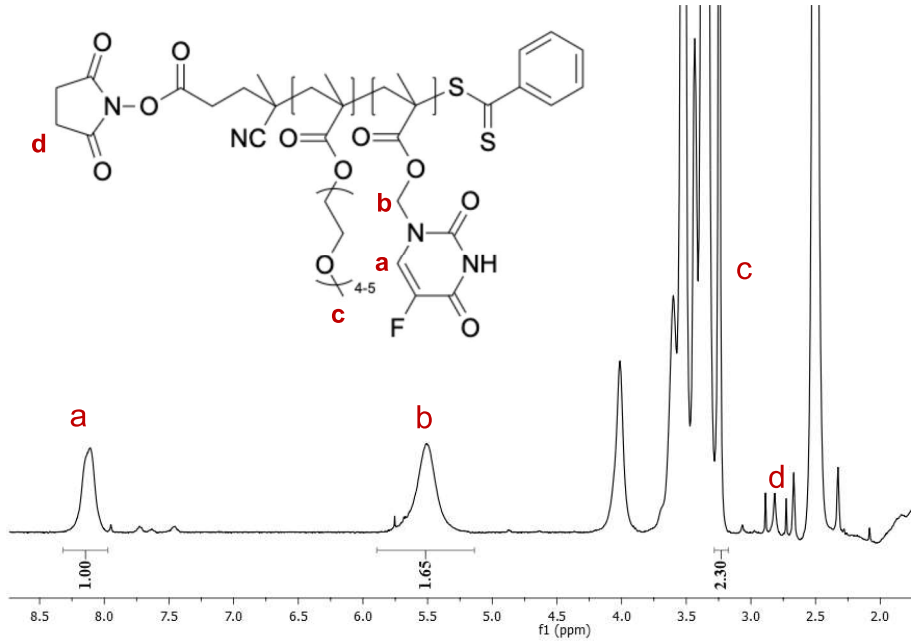

Figure 4.12. ^{1}H-NMR spectrum of NHS-p(OEGMEMA)-*b*-p(5FUMA).

The number of 5FUMA repeating units was determined by comparing the integration of the proton resonances at 8.1 ppm and 3.3 ppm, which are due to a proton in the 5FUMA ring and three terminal methyl ether protons of OEGMEMA, respectively. 38 5FUMA repeating units in p(OEGMEMA)-*b*-p(5FUMA) and 32 5FUMA repeating units in NHS-p(OEGMEMA)-*b*-p(5FUMA) were obtained. GPC molecular weight (Mn) and PDI values for p(OEGMEMA)-*b*-p(5FUMA) and NHS-p(OEGMEMA)-*b*-p(5FUMA) were found to be 51.03 kDa, 1.153 and 52.83 kDa, 1.113, respectively.

4.4. Synthesis and Characterization of cRGDfK-p(OEGMEMA)-*b*-p(5FUMA) Block Copolymer

To obtain a block copolymer with the cyclic peptide cRGDfK at the hydrophilic end group, the high yield reaction between NHS activated ester and amines was utilized. The NHS ester was present on the initial chain transfer agent SCPDB, so that the homopolymer NHS-p(OEGMEMA) and block copolymer NHS-p(OEGMEMA)-*b*-p(5FUMA) synthesized from this CTA also possessed the NHS ester.

Post-polymerization modification of the NHS ester at the carboxyl end of the block copolymer NHS-p(OEGMEMA)-*b*-p(5FUMA) was performed by reacting the NHS ester with the primary amine of the peptide under alkaline conditions to yield a chemically stable amide bond between the polymer and peptide, as shown in Figure 4.13, and the targeted block copolymer cRGDfK-p(OEGMEMA)-*b*-p(5FUMA) was obtained.

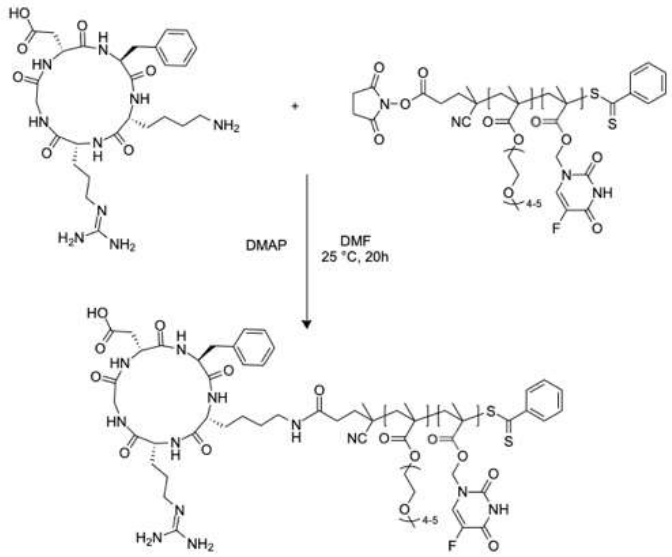

Figure 4.13. Synthesis of cRGDfK-p(OEGMEMA)-*b*-p(5FUMA).

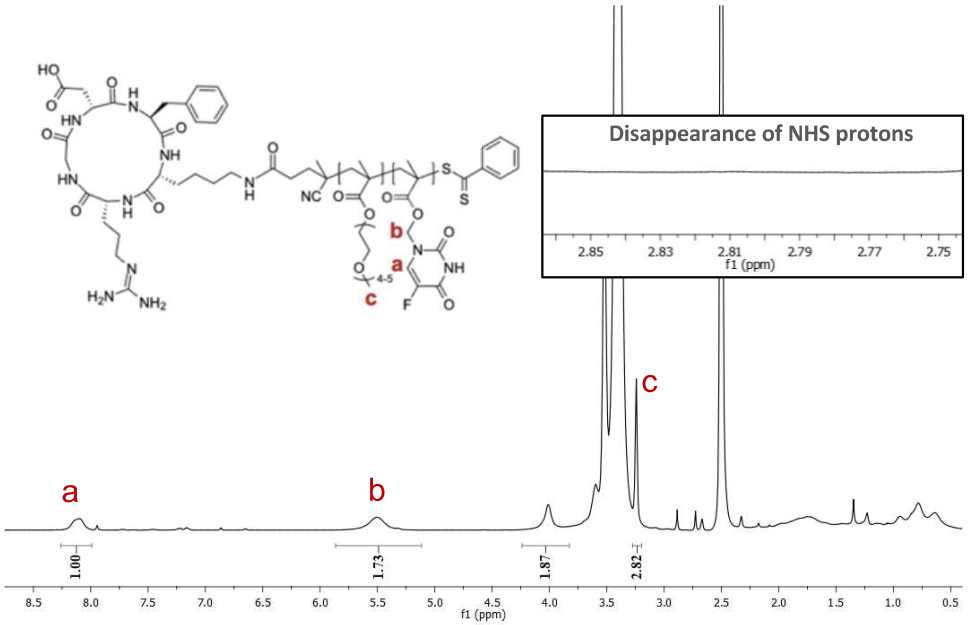

Figure 4.14. ^{1}H-NMR spectrum of cRGDfK-p(OEGMEMA)-*b*-p(5FUMA).

In the ^{1}H-NMR spectrum of cRGDfK-p(OEGMEMA)-*b*-p(5FUMA) in DMSO (Figure 4.14), it is seen that proton resonances belonging to the NHS group at 2.88 ppm, which were present in the ^{1}H-NMR spectrum of NHS-p(OEGMEMA)-*b*-p(5FUMA) (Figure 4.12), disappear as a result of the cleaving of NHS. This disappearance of NHS proton resonances, along with the presence of new proton resonances between 6.50-7.50 ppm due to phenylic protons of cRGDfK proves the successful attachment of the peptide on all polymer chains.

The molecular weight (Mn) values of the block copolymers were determined by using the repeating units of the OEGMEMA and 5FUMA groups, as integrated from their ^{1}H-NMR spectra. GPC traces of polymers also indicate increased molecular weights after the polymerization of 5FUMA, as well as similar molecular weights for non-targeted, NHS functionalized and cRGDfK targeted block copolymers (Figure 4.15), but give inaccurate Mn values for block copolymers, possibly due to the difference between the structures of the polymers and the standards used in the calibration curve of the instrument. The number of repeating units of OEGMEMA and 5FUMA obtained from ^{1}H-NMR spectra Mn values calculated using these repeating units, and Mn and PDI values obtained from GPC are summarized in Table 4.1.

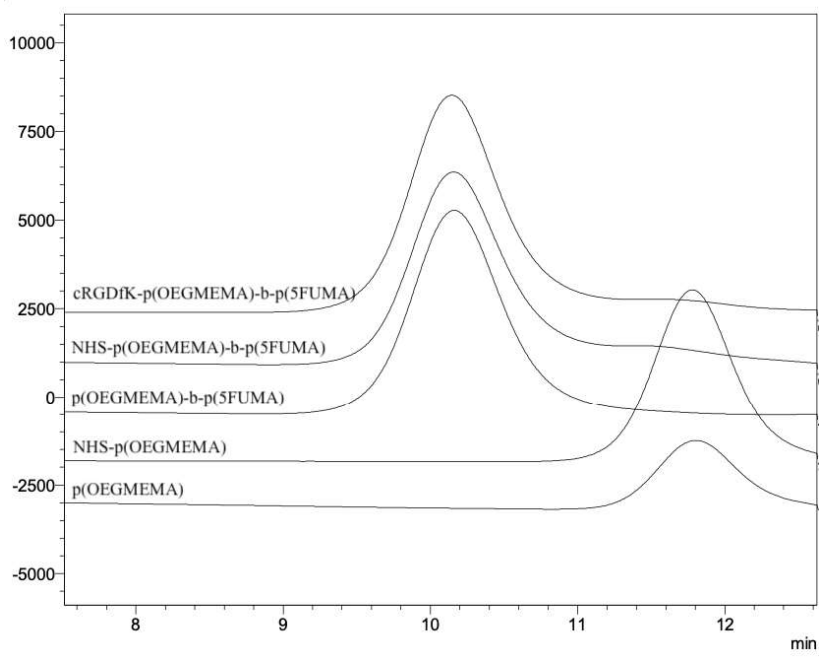

Figure 4.15. GPC traces of all synthesized polymers.

Table 4.1. Repeating unit numbers and molecular weight values of synthesized polymers.

	OEGMEMA Repeating Units	5FUMA Repeating Units	Mn* (g/mol)	5-FU wt. %	Mn** (kDa)	PDI**
p(OEGMEMA)	21	-	6500	-	5.83	1.186
NHS-p(OEGMEMA)	24	-	7500	-	6.05	1.210
p(OEGMEMA)-*b*-p(5FUMA)	21	38	15200	33	51.03	1.153
NHS-p(OEGMEMA)-*b*-p(5FUMA)	24	32	14800	28	52.83	1.113
cRGDfK-p(OEGMEMA)-*b*-p(5FUMA)	24	32	15400	27	53.52	1.113

* Calculated using the ^{1}H-NMR proton resonance integration values

** Obtained by gel permeation chromatography (GPC) using poly(methylmethacrylate) standarts.

4.5. Critical Micelle Concentration (CMC) of Block Copolymers

Critical micelle concentration of a polymer (CMC) is the concentration of the polymer required to self-assemble into micelles in an aqueous solution. To determine the CMC of the polymers, pyrene was used as the fluorescence probe. Various samples containing pyrene and different concentrations of the block copolymer p(OEGMEMA)-*b*-p(5FUMA) were prepared by mixing in acetone, adding water, and evaporating acetone overnight. During evaporation of the organic solvent, micelles begin to form if the concentration of the polymers is above the CMC value. As these micelles form, pyrene, a hydrophobic fluorescent dye, is encapsulated in the hydrophobic core of micelles, resulting in the transfer of pyrene from a polar to a nonpolar microenvironment. This transfer causes a major change in the I_{338}/I_{334} value of pyrene in solution, and a steep increase in this ratio was used in the calculation of the CMC value. The intersection of trendlines of intensity ratios that are relatively constant and those that are rapidly increasing was determined to calculate the CMC value for the non-targeted block copolymer, p(OEGMEMA)-*b*-p(5FUMA), as 1.33 x 10^{-6} M, as shown in Figure 4.16.

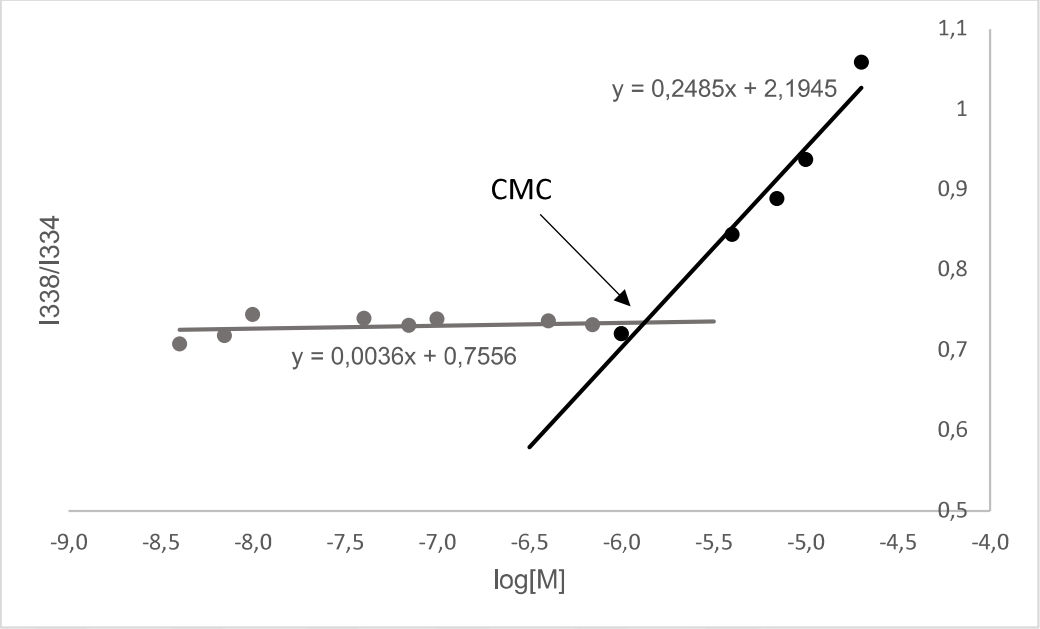

Figure 4.16. CMC graph of p(OEGMEMA)-*b*-p(5FUMA).

Because the block copolymers p(OEGMEMA)-*b*-p(5FUMA) and cRGDfK-p(OEGMEMA)-*b*-p(5FUMA) had similar OEGMEMA and 5FUMA repeating units and molecular weights, as shown in Table 4.1, their CMC values were predicted to be similar as well. Additionally, since targeted micelles were prepared from a combination of targeted and non-targeted block copolymers, the CMC of the targeted block copolymer cRGDfK-p(OEGMEMA)-*b*-p(5FUMA) alone was not measured.

4.6. Formation of Non-Targeted and Targeted Polymeric Micelles

Due to the hydrophilic OEGMEMA segment and the 5-FU bearing hydrophobic segment, the block copolymers showed amphiphilic properties, including the formation of micellar polymeric nanoparticles through self-assembly in aqueous environment, as proven by CMC experiments. As the self-assembly process takes place, the presence of the ribociclib drug in solution resulted in its encapsulation in the hydrophobic core of the micellar nanoparticles (Figure 4.17 and Figure 4.18).

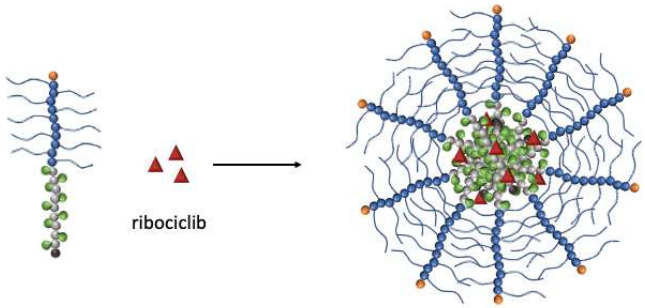

Figure 4.17. Formation of ribociclib loaded non-targeted polymeric micelles (FUMi-R) using p(OEGMEMA)-*b*-p(5FUMA) and ribociclib.

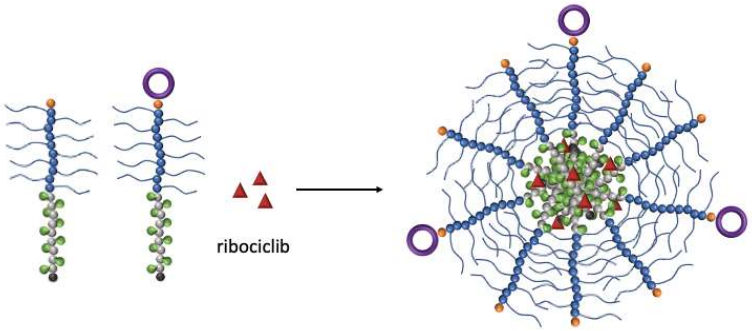

Figure 4.18. Formation of ribociclib loaded targeted polymeric micelles (RGD-FUMi-R) using p(OEGMEMA)-*b*-p(5FUMA), cRGDfK-p(OEGMEMA)-*b*-p(5FUMA) and ribociclib.

Cosolvent evaporation was occupied for micelle preparation, where the components were mixed in organic solvent, and after dropwise addition of distilled water, organic solvent was evaporated to give micellar nanoparticles. To form ribociclib loaded non-targeted micellar nanoparticles (FUMi-R), p(OEGMEMA)-*b*-p(5FUMA) and ribociclib were used (Figure 4.17), and for ribociclib loaded targeted micellar nanoparticles (RGD-FUMi-R), ribociclib and a mixture of cRGDfK-p(OEGMEMA)-*b*-p(5FUMA) and p(OEGMEMA)-*b*-p(5FUMA) (1/4, w/w) were used (Figure 4.18). For formation of non-targeted micelles (FUMi) and targeted micelles (RGD-FUMi) that don't contain ribociclib, the same procedure was followed with the polymers without ribociclib addition.

Micelles with a drug loading (DL) of 5.32 ± 0.14 wt.% ribociclib were obtained, and the encapsulation efficiency (EE) of ribociclib in micelles was found to be 97.19 ± 0.12 %.

Micelle formation was seen by analysis of samples using dynamic light scattering (DLS). DLS measurements were taken to both observe the formation, and determine the average size and PDI of micellar nanoparticles. Micelles with average sizes around 10 – 20 nm by volume were obtained, as listed in Table 4.2 with the PDI values, and seen in Figure 4.19 in the size distribution graph of each micelle.

Table 4.2. Average sizes and PDI values of all micellar nanoparticles.

	Average Size by Volume (nm) *	PDI*
FUMi	11.28 ± 1.37	0.543 ± 0.005
FUMi-R	19.32 ± 1.21	0.517 ± 0.030
RGD-FUMi	17.00 ± 0.71	0.552 ± 0.007
RGD-FUMi-R	22.44 ± 0.56	0.530 ± 0.002

* Obtained by DLS measurements

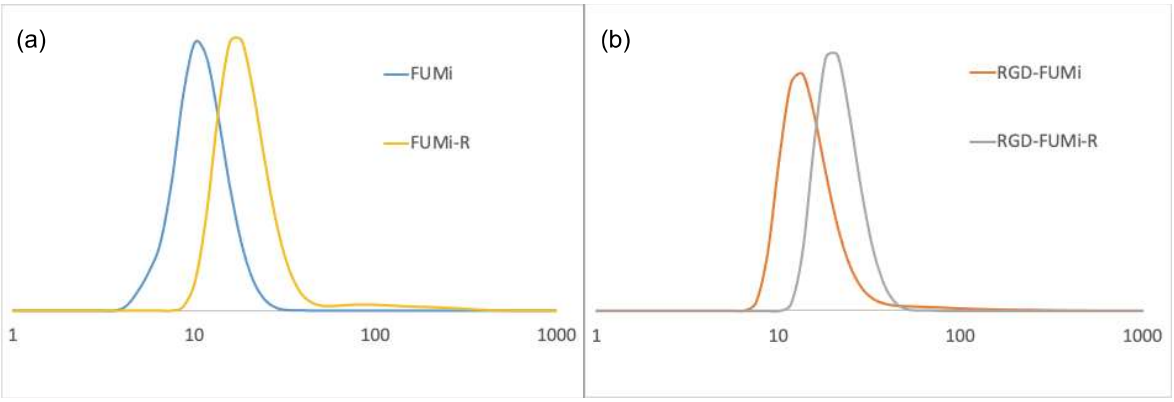

Figure 4.19. Size distributions of (a) FUMi (blue) and FUMi-R (yellow) (b) RGD-FUMi (orange) and RGD-FUMi-R (grey) by volume.

The increased sizes of both RGD-FUMi-R and FUMi-R compared to RGD-FUMi and FUMi respectively, as seen in Table 4.2 and in their size distributions by volume in Figure 4.19, was attributed to the encapsulation of ribociclib in the hydrophobic core.

4.7. Stability of Polymeric Micelles

Stability of polymeric micelles upon ultra-dilution is an important aspect, since the micelles go through similar dilutions when injected into the bloodstream. To measure the stability of micelles upon ultra-dilution, FUMi-R containing 1 x 10^{-5} M p(OEGMEMA)-b-p(5FUMA) were prepared by following to the procedure mentioned earlier, and subjected to ultra-dilution by diluting two-fold with distilled water several times to observe the dilution factor up to which the micelles remain intact.

The micelles were found to be very stable upon dilution. It was observed that during dilution, the average size of micelles generally increased from around 20 nm to a maximum of around 35 nm (Figure 4.20). At 1024x dilution, no micellar nanoparticles remained in solution, indicating the disassembly of the micelles back to its components, block copolymers and free ribociclib .

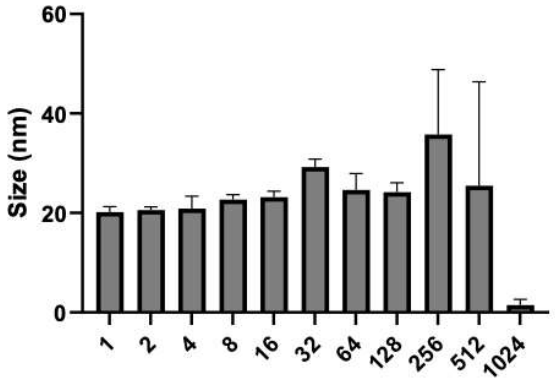

Figure 4.20. Stability of FUMi-R upon dilution.

The stability of micellar nanoparticles upon the lyophilization of micelle solutions was also investigated. For this, micelle solutions were prepared according to the procedure mentioned earlier, DLS and drug loading measurements were taken, and the solutions were freeze-dried. Lyophilized micellar nanoparticles were then dissolved in water, DLS measurements were taken, and micelles were filtered for drug loading analysis.

As seen in Table 4.3 and Figure 4.21, FUMi-R micelles were found to be stable after lyophilization. Their average sizes increased slightly compared to before the lyophilization, and percent drug loading of micelles decreased minimally.

Table 4.3. Drug loading and average sizes of FUMi-R before and after lyophilization.

	Before lyophilization		After lyophilization	
	Drug Loading (%)	Average Size (nm)	Drug Loading (%)	Average Size (nm)
FUMi-R	5.69	17.08	5.12	20.13

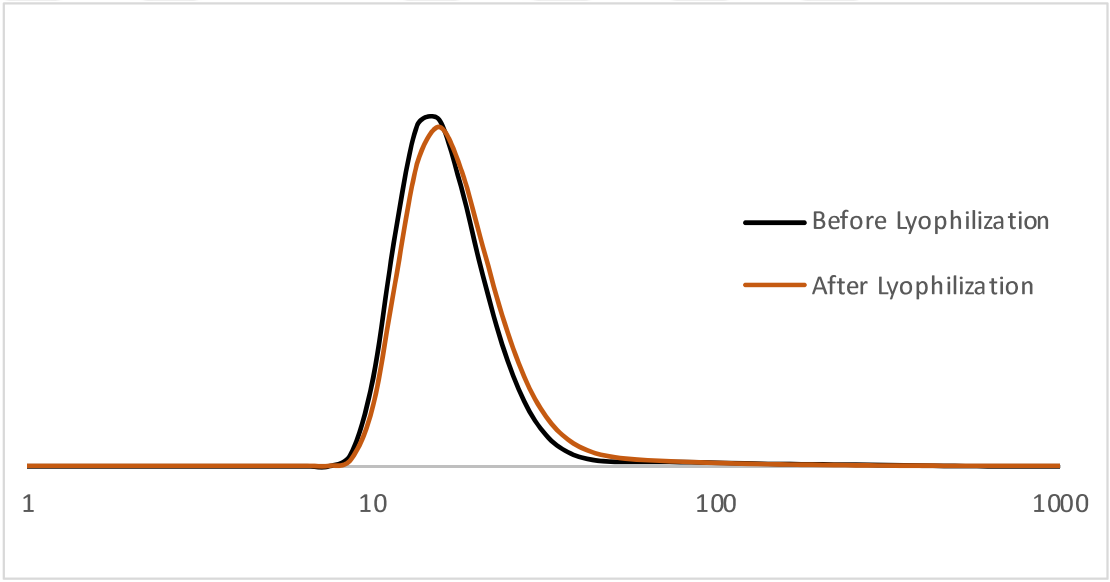

Figure 4.21. Size distribution of FUMi-R by volume before (black) and after (orange) lyophilization.

It is a valuable finding that the polymeric micelles can be reconstituted after freeze drying, since this property could potentially simplify the micelle preparation in later studies without the need to prepare micelle solutions from scratch.

4.8. *In vitro* Drug Release from Polymeric Micelles

Ribociclib was released from FUMi-R via dialysis in buffers with acidic (Acetate Buffer, pH 5.5), basic (Carbonate Buffer, pH 10.5), and physiological (PBS, pH 7.4) pH values, and the cumulative ribociclib release in each of these conditions is shown in Figure 4.22. Release of ribociclib was slow at pH 7.4, and much faster at pH 5.5 or 10.5, reaching saturation after 8 hours. These results indicate that the micellar nanoparticles are effective carriers of cytotoxic drugs, since they exhibit controlled drug release in the pH of blood or similar body regions, while providing a burst release of the drug in acidic environments, similar to the tumor microenvironment.

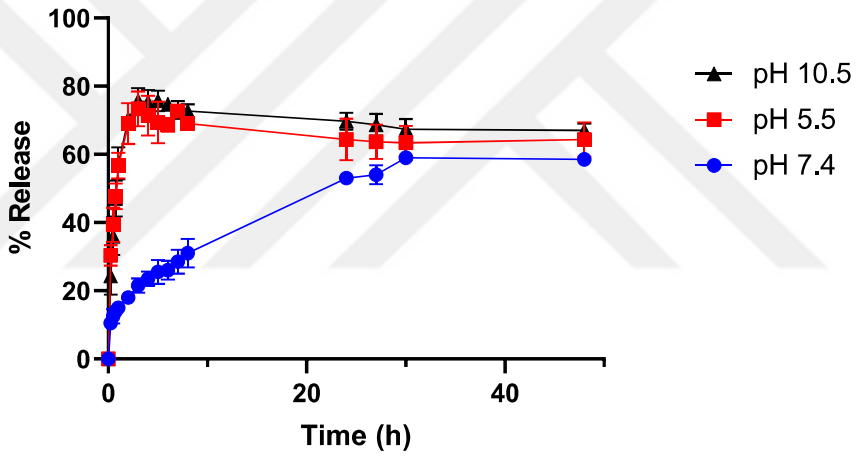

Figure 4.22. Cumulative Ribociclib release from FUMi-R at pH 5.5, 7.4 and 10.5.

It was observed that 5-FU release was very slow in each pH, and in the cases of pH 5.5 and 7.4, no significant 5-FU release could be observed. The released 5-FU could be detected only at pH 10.5, but the release was still very slow and total drug release was less than 5 % even after 120 hours, as seen in Figure 4.23, which suggests that even stronger basic conditions may be required to completely break the ester linkages between the drug and polymer backbone.

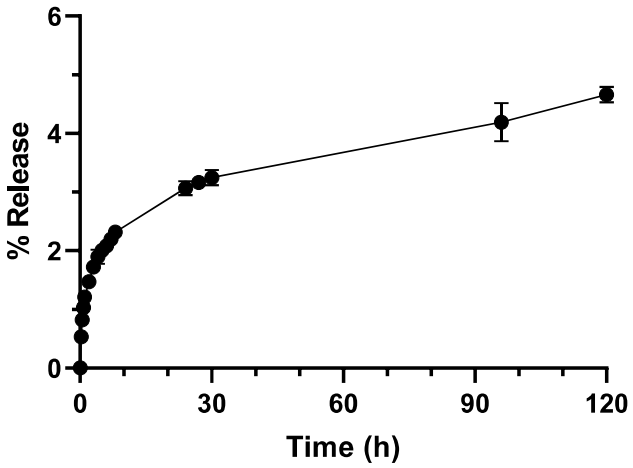

Figure 4.23. Cumulative 5-Fluorouracil release from FUMi-R at pH 10.5.

In order to reach more solid conclusions about 5-FU release from block copolymers, release of 5-FU from the monomer 5FUMA was performed by preparing solutions of 5FUMA in buffer solutions and shaking at 37 °C until analysis using LC-MS. It was observed that all of the 5-FU was cleaved from the monomer after 24 hours at pH 10.5, whereas slower release was seen in the case of pH 7.4, and an even slower release at pH 5.5, as seen in Figure 4.24.

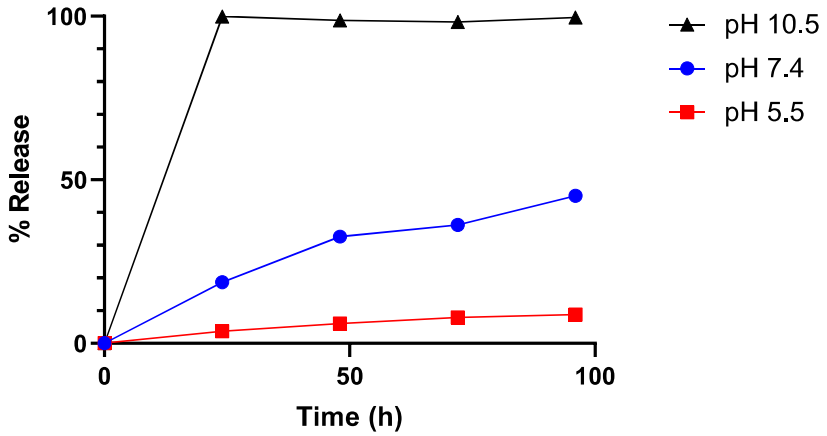

Figure 4.24. Release of 5-FU from 5FUMA at pH 5.5, 7.4 and 10.5.

Since complete cleaving of the ester bond to release 5-FU was observed when 5FUMA was introduced to basic conditions, it was concluded that 5-FU was not easily cleaved from the backbone of the block copolymers in buffer solutions possibly because the cleavable ester bond between polymer and 5-FU is very close to the backbone, and because the hydrophobic chain containing 5-FU is not in direct contact with the buffer solutions since it is forming the core of the micelles used in the release studies.

4.9. *In vitro* Cytotoxicity of Polymeric Micelles on Neuroendocrine Tumor Cells

It was reported in literature that, in addition to the antitumor activity of ribociclib on neuroendocrine tumors [79], ribociclib and 5-FU have shown synergistic effect on colorectal cancer cell lines [90] and some neuroendocrine tumor cell lines [91]. To find out if these drugs demonstrate synergy on NCI-H727 human lung neuroendocrine tumor cells, cells were treated with varying concentrations of ribociclib, 5-FU or their combination, and their viabilities were assessed via CCK-8 assay. The results, shown in Figure 4.25, revealed that specific combinations of ribociclib and 5-FU concentrations resulted in decreased viability of NCI-H727 cells compared to 5-FU or ribociclib alone.

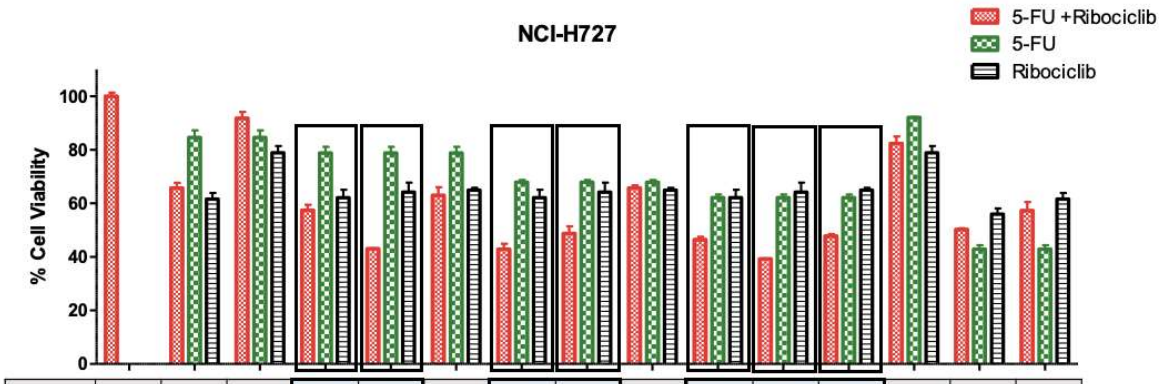

5-FU (M)	0	1 x 10^{-6}	1 x 10^{-6}	2 x 10^{-6}	2 x 10^{-6}	2 x 10^{-6}	3 x 10^{-6}	3 x 10^{-6}	3 x 10^{-6}	5 x 10^{-6}	5 x 10^{-6}	5 x 10^{-6}	1 x 10^{-7}	1 x 10^{-5}	1 x 10^{-5}
Ribociclib (M)	0	1 x 10^{-6}	1 x 10^{-7}	2 x 10^{-6}	3 x 10^{-6}	5 x 10^{-6}	2 x 10^{-6}	3 x 10^{-6}	5 x 10^{-6}	2 x 10^{-6}	3 x 10^{-6}	5 x 10^{-6}	1 x 10^{-7}	1 x 10^{-5}	1 x 10^{-6}
Combination Index (CI)	-	0.957	452.358	**0.519**	**0.124**	2.229	**0.168**	**0.301**	4.247	**0.354**	**0.207**	**0.455**	6.647	1.140	1.527

Figure 4.25. Viability of NCI-H727 cells treated with 5-FU + Ribociclib (red), 5-FU (green), and Ribociclib (black). (CI < 1 : synergistic effect, CI = 1 : additive effect, CI > 1 : antagonistic effect.)

Cytotoxicity of micelles and free drugs on NCI-H727 human lung neuroendocrine tumor cells as well as BE(2)-C human neuroblastoma cells were determined via CCK-8 studies to determine the efficacy of the antitumor effect of micelles on neuroendocrine tumor cells. The results are shown in Figure 4.26 and Figure 4.27.

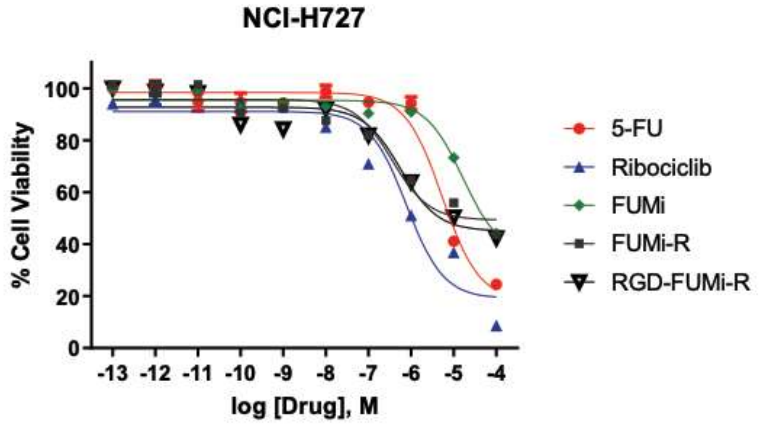

	5-FU	Ribociclib	FUMi	FUMi-R	RGD-FUMi-R
EC_{50}	5.4×10^{-6}	7.8×10^{-7}	1.6×10^{-5}	3.5×10^{-7}	5.7×10^{-5}

Figure 4.26. Effect of free 5-FU, free ribociclib, FUMi, FUMi-R and RGD-FUMi-R on viability of NCI-H727 cells, and their EC_{50} values in mol/L.

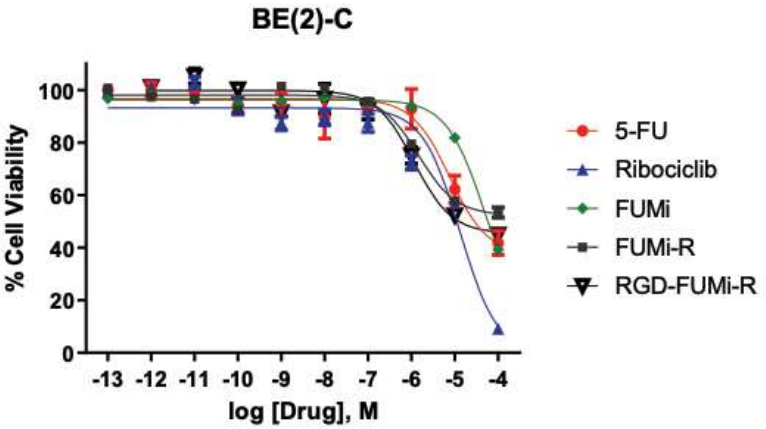

	5-FU	Ribociclib	FUMi	FUMi-R	RGD-FUMi-R
EC_{50}	7.6×10^{-6}	1.3×10^{-5}	4.8×10^{-5}	1.5×10^{-6}	1.2×10^{-6}

Figure 4.27. Effect of free 5-FU, free ribociclib, FUMi, FUMi-R and RGD-FUMi-R on viability of BE(2)-C cells, and their EC_{50} values in mol/L.

FUMi-R and RGD-FUMi-R showed similar cytotoxicity to each other and free drugs, indicating successful decrease in the proliferation using micelles. Due to the 5-FU *in vitro* release observations, cytotoxicity of FUMi as well as FUMi-R and RGD-FUMi-R was assessed in order to see whether the 5-FU molecules that are conjugated in the hydrophobic block of the block copolymers can cleave and cause cytotoxic effect on neuroendocrine cancer cell lines without the second drug. It was observed, as seen in Figure 4.26 and Figure 4.27, that although FUMi-R and RGD-FUMi-R were more toxic to cancer cells, FUMi was also able to decrease cell viability at relatively higher concentrations. This result proves that although 5-FU could not be released in *in vitro* release studies, in cellular media, some of the drug is able to cleave from the backbone of the polymer and cause toxic effect.

4.10. Internalization of Polymeric Micelles in Neuroendocrine Tumor Cells

It was established in literature that some NETs overexpress integrin $\alpha_v\beta_3$ receptors, enabling the use of integrin $\alpha_v\beta_3$ targeting cyclic peptides in NET internalization [91, 92]. So far, internalization of imaging agents for the diagnosis of NETs have largely been the focus for the use of such peptides, and often in combination with somatostatin receptor targeting peptides, but drug delivery can also be enhanced using this property of NETs.

In the scope of this project, Nile red (NR) was used as a probe for the internalization studies of non-targeted and targeted polymeric micelles in NCI-H727 and BE(2)-C cell lines to visualize the targeting ability of targeted micelles. The fluorescence images of cells after treatment with either free NR, targeted NR loaded micelles (RGD-FUMi-NR), non-targeted NR loaded micelles (FUMi-NR) or free cRGDfV peptide along with targeted NR loaded micelles were taken after 1h and 3h of incubation at 37 °C followed by nuclei staining with DAPI. Merged images and fluorescence intensities of NCI-H727 cells are shown in Figure 4.28 and Figure 4.29, and those of BE(2)-C cells are shown in Figure 4.30 and Figure 4.31, respectively.

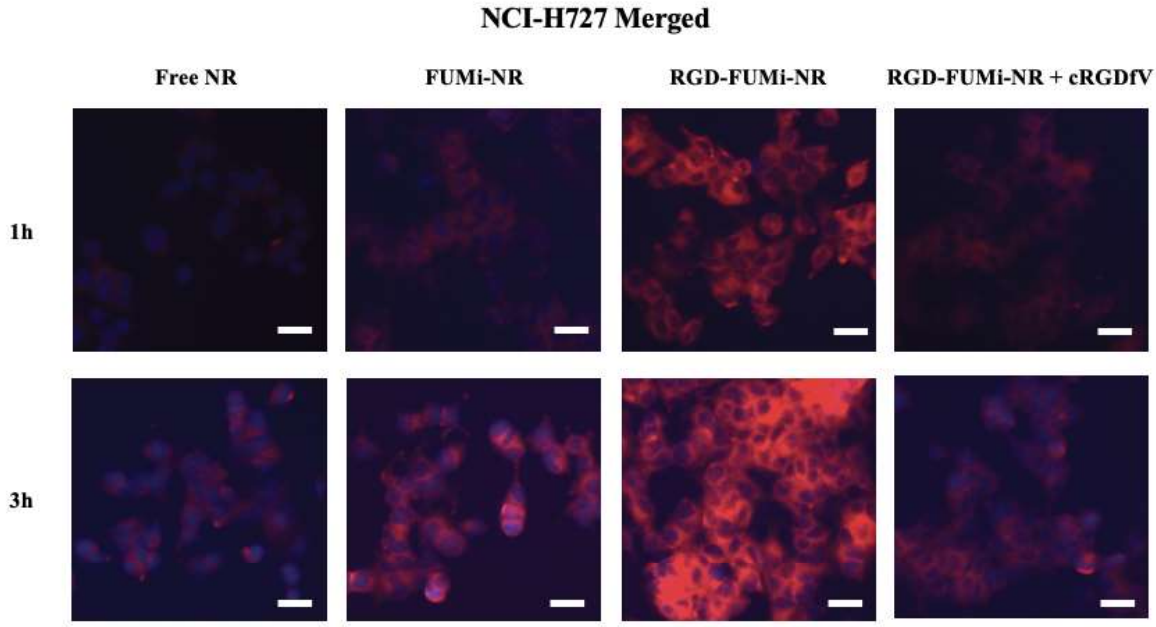

Figure 4.28. Fluorescence images of NCI-H727 cells after treatment with controls and micelle solutions and incubation at 37 °C for 1h and 3h.

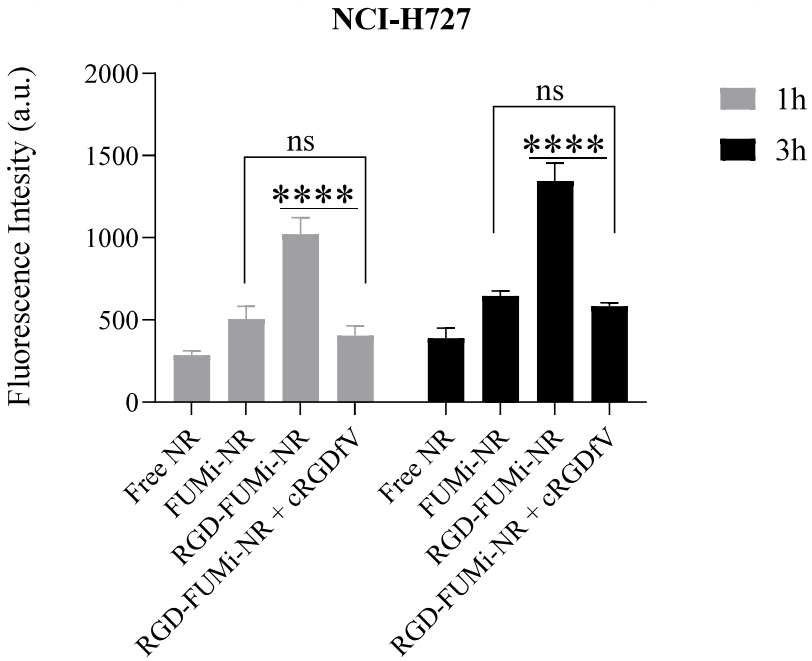

Figure 4.29. Fluorescence intensities of NCI-H727 cells after treatment with controls and micelle solutions and incubation at 37 °C for 1h and 3h.

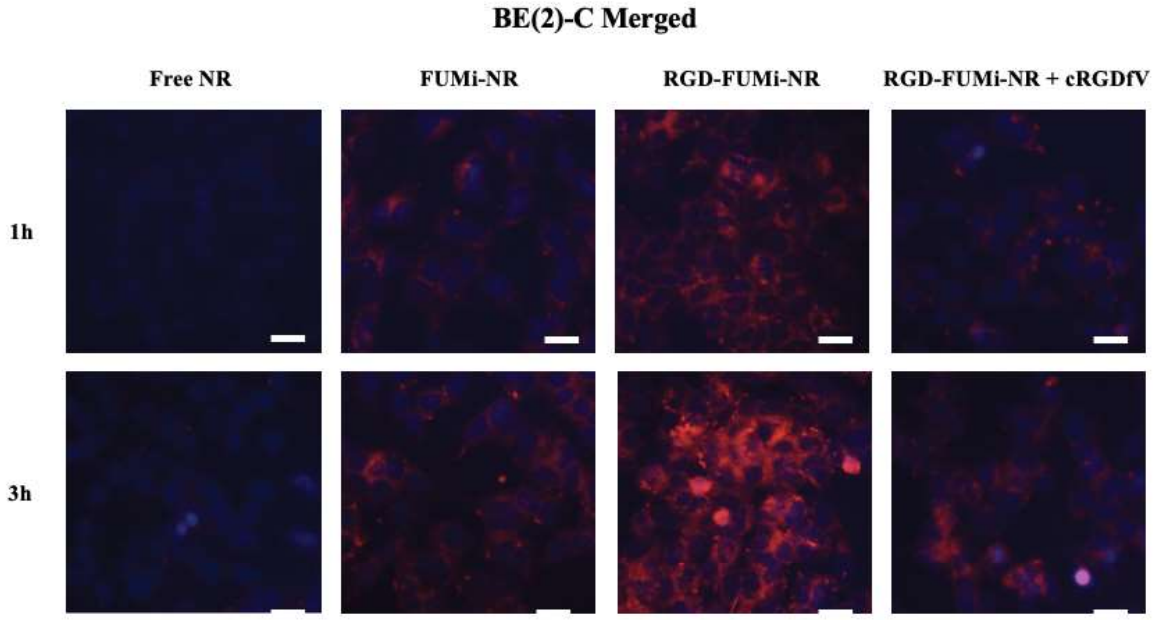

Figure 4.30. Fluorescence images of BE(2)-C cells after treatment with controls and micelles and incubation at 37 °C for 1h and 3h.

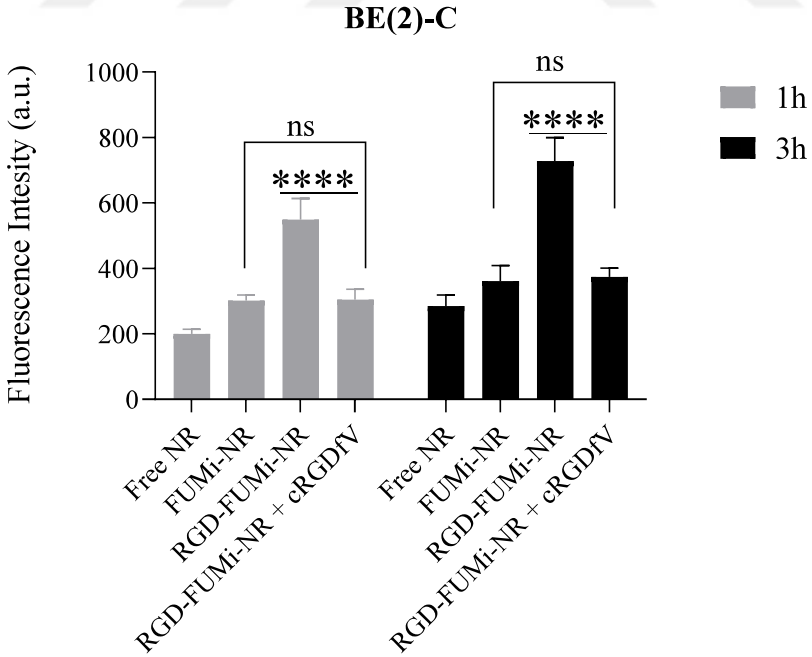

Figure 4.31. Fluorescence intensities of BE(2)-C cells after treatment with controls and micelle solutions and incubation at 37 °C for 1h and 3h.

In both NCI-H727 and BE(2)-C cells, enhanced cellular uptake was observed when the cells were treated with RGD-FUMi-NR, compared to FUMi-NR, as seen from the significantly increased fluorescence intensities of cells after RGD-FUMi-NR treatment in Figure 4.28 and Figure 4.30. Cells were also treated with free NR as a control, which was internalized in small amounts in the cells, as seen from the fluorescence images and fluorescence intensity values, while still showing less uptake than both RGD-FUMi-NR and FUMi-NR in both cell lines. This indicates that internalization is increased due to the micellar formulation, which acts as a carrier for hydrophobic molecules such as NR.

Another control experiment, involving competitive binding, was performed by treating the cells with free cRGDfV and RGD-FUMi-NR simultaneously to block their integrin $\alpha_v\beta_3$ receptors with the free peptide, and determine whether the enhanced internalization seen in the case of RGD-FUMi-NR treatment is in fact due to the presence of cRGDfK peptide on the corona of micelles. In both cells, the fluorescence intensities of cells after treatment with cRGDfV and RGD-FUMi-NR were found to be significantly less than those treated directly with RGD-FUMi-NR only, and no significant difference in fluorescence intensities was observed compared to FUMi-NR treatment (Figure 4.28 and Figure 4.30). These results present proof that the presence of cRGDfK on the micelles is the main reason for the increased cellular uptake of RGD-FUMi-NR, supporting the hypothesis that actively targeting the $\alpha_v\beta_3$ receptors of NETs via cRGDfK functionalized drug delivery systems is a viable treatment option.

Overall, internalization experiments indicated that micellar delivery of small hydrophobic molecules to NET cell lines leads to enhanced cellular uptake compared to free small hydrophobic molecules, and that the presence of the targeting peptide, cRGDfK, on micelle corona is able to increase the uptake of micelles, and therefore the cargo molecules, in these cell lines.

5. CONCLUSION

In this project, a targeted drug delivery system for the codelivery of 5-FU and ribociclib to neuroendocrine tumors was developed. A 5-FU monomer, 5FUMA was successfully synthesized and then polymerized with the synthesized macro chain transfer agents NHS-p(OEGMEMA) and p(OEGMEMA) via RAFT polymerization to yield a non-targeted and an NHS functionalized block copolymer. The NHS functionalized block copolymer was further reacted with the cRGDfK peptide via activated ester-amine chemistry to obtain the targeted block copolymer. Non-targeted and targeted polymeric micelles loaded with the CDK4/6 inhibitor ribociclib, FUMi-R and RGD-FUMi-R, were prepared using these amphiphilic polymers, and their sizes, drug loading, and stability were determined. Micelles with a ribociclib loading around 5 % were found to be around 20 nm in size, and were quite stable upon dilution. Drug release studies indicated that at physiological pH, ribociclib was released slowly from micelles, whereas under acidic or basic conditions, release of ribociclib was very fast. 5-FU was only able to cleave in very small amounts from the construct in any pH, although a relatively increased release profile was observed in basic buffers. Still, FUMi, without ribociclib, showed some cytotoxicity towards two neuroendocrine tumor cell lines, indicating that some 5-FU is released in cellular media or inside the cells. The cytotoxic effect of FUMi-R and RGD-FUMi-R were also determined, and these micelles showed EC_{50} values that were lower than that of FUMi and similar to ribociclib, pointing to successful decrease in proliferation of neuroendocrine tumor cells. Cellular uptake of FUMi and RGD-FUMi on the same cell lines were performed, and it was concluded that targeted micelles are internalized faster than non-targeted ones, supporting the hypothesis presented in this study that targeted drug delivery to NETs via cRGDfK functionalized drug delivery systems is a powerful strategy. Further research is needed to obtain faster 5-FU release from the block copolymer by introducing stimuli-sensitive linkers between 5-FU and the polymer backbone, and to determine the *in vivo* pharmacokinetics of the targeted micelles obtained in this project. Future work also includes the synthesis of Trastuzumab and Cetuximab bearing micelles, and determination of their cytotoxic effects, internalizations, and *in vivo* pharmacokinetics on NET cell lines, as well as comparison of these effects with the results obtained in the current project.

REFERENCES

1. National Cancer Institute, “What is cancer?”, 2021, https://www.cancer.gov/about-cancer/understanding/what-is-cancer, accessed on July 6, 2023.

2. Global Cancer Observatory, “All Cancers”, 2020, https://gco.iarc.fr/today/data/factsheets/cancers/39-All-cancers-fact-sheet.pdf, accessed on July 6, 2023.

3. Global Cancer Observatory, “Cancer Tomorrow”, 2020, https://gco.iarc.fr/tomorrow/en/dataviz/isotype, accessed on July 6, 2023.

4. Morales-Cruz, M., Y. Delgado, B. Castillo, C. M. Figueroa, A. M. Molina, A. Torres, M. Milián, and K. Griebenow, “Smart Targeting to Improve Cancer Therapeutics" *Drug Design, Development and Therapy*, Vol. 13, pp. 4935–4955 , 2019.

5. Cho, K., X. Wang, S. Nie, Z. G. Chen, and D. M. Shin, "Therapeutic Nanoparticles for Drug Delivery in Cancer", *Clinical Cancer Research*, Vol. 14, No. 5, pp. 1310–1316, 2008.

6. Edis, Z., J. Wang, M. K. Waqas, M. Ijaz, and M. Ijaz, “Nanocarriers-Mediated Drug Delivery Systems for Anticancer Agents: An Overview and Perspectives”, *International Journal of Nanomedicine*, Vol. 2021, No. 16, pp. 1313–1330 , 2021.

7. Jain, K. K., *Drug Delivery Systems*, Third Edition, Humana, New Jersey, 2010.

8. Kim, T. Y., D. W. Kim, J. Y. Chung, S. G. Shin, S. C. Kim, D. S Heo, N. K. Kim, and Y. J. Bang, “Phase I and Pharmacokinetic Study of Genexol-PM, a Cremophor-Free, Polymeric Micelle-Formulated Paclitaxel, in Patients with Advanced Malignancies”, *Clinical Cancer Research*, Vol. 10, No. 11, pp. 3708–3716, 2004.

9. Wang-Gillam, A., C. P. Li, G. Bodoky, A. Dean, Y. S. Shan, G. Jameson, T. Macarulla, K. H. Lee, D. Cunningham, J. F. Blanc, R. A. Hubner, C. F. Chiu, G. Schwartsmann, J. T. Siveke, F. Braiteh, B. Belanger, N. Dhindsa, E. Bayever, D. D. Von Hoff, and L. T. Chen, "Nanoliposomal Irinotecan with Fluorouracil and Folinic Acid in Metastatic Pancreatic Cancer After Previous Gemcitabine-Based Therapy (NAPOLI-1): A Global, Randomised, Open-Label, Phase 3 Trial", *Lancet*, Vol. 387, No. 10018, pp. 545–557, 2015.

10. Gradishar W. J., S. Tjulandin, N. Davidson, H. Shaw, N. Desai, P. Bhar, M. Hawkins, and J. O'Shougnessy, "Phase III Trial of Nanoparticle Albumin-Bound Paclitaxel Compared with Polyethylated Castor Oil-Based Paclitaxel in Women with Breast Cancer", *Journal of Clinical Oncology*, Vol. 23, No. 31, pp. 7794–7803, 2005.

11. Çırpanlı, Y., E. Allard, C. Passirani, E. Bilensoy, L. Lemaire, S. Çalış, and J. Benoit, "Antitumoral Activity of Camptothecin-Loaded Nanoparticles in 9L Rat Glioma Model", *International Journal of Pharmaceutics*, Vol. 403, No. 1–2, pp. 201–206, 2011.

12. Guo, J., X. Gao, L. Su, H. Xia, G. Gu, Z. Pang, X. Jiang, L. Yao, J. Chen, and H. Chen, "Aptamer-Functionalized PEG–PLGA Nanoparticles for Enhanced Anti-Glioma Drug Delivery", *Biomaterials*, Vol. 32, No. 31, pp. 8010–8020, 2011.

13. Yuan, J., D. ZhuGe, M. Tong, M. Lin, X. Xu, X. Tang, Y. Zhao, and H. Xu, "pH-Sensitive Polymeric Nanoparticles of mPEG-PLGA-PGlu with Hybrid Core for Simultaneous Encapsulation of Curcumin and Doxorubicin to Kill the Heterogeneous Tumour Cells in Breast Cancer", *Artificial Cells, Nanomedicine, and Biotechnology*, Vol. 46, No. S1, pp. S302–S313, 2018.

14. Hu, D., L. Chen, Y. Qu, J. Peng, B. Chu, K. Shi, Y. Hao, L. Zhong, M. Wang, and Z. Qian, "Oxygen-generating Hybrid Polymeric Nanoparticles with Encapsulated Doxorubicin and Chlorin e6 for Trimodal Imaging-Guided Combined Chemo-Photodynamic Therapy", *Theranostics*, Vol. 8, No. 6, pp. 1558–1574, 2018.

15. Zhu, D., W. Tao, H. Zhang, G. Liu, T. Wang, L. Zhang, X. Zeng, and L. Mei, "Docetaxel (DTX)-Loaded Polydopamine-Modified TPGS-PLA Nanoparticles as a Targeted Drug Delivery System for the Treatment of Liver Cancer", *Acta Biomaterialia*, Vol. 30, pp. 144–154, 2016.

16. Maeda H., and Y. Matsumura, "Tumoritropic and Lymphotropic Principles of Macromolecular Drugs.", *Critical Reviews in Therapeutic Drug Carrier Systems*, Vol. 6, No. 3, pp. 193–210, 1989.

17. Maeda, H., H. Nakamura, and J. Fang, "The EPR Effect for Macromolecular Drug Delivery to Solid Tumors: Improvement of Tumor Uptake, Lowering of Systemic Toxicity, and Distinct Tumor Imaging *in vivo*", *Advanced Drug Delivery Reviews*, Vol. 65, No. 1, pp. 71–79, 2013.

18. Jain, R. K., "Transport of Molecules, Particles, and Cells in Solid Tumors", *Annual Review of Biomedical Engineering*, Vol. 1, No. 1, pp. 241–263, 1999.

19. Jain R. K., and T. Stylianopoulos, "Delivering Nanomedicine to Solid Tumors", *Nature Review Clinical Oncology*, Vol. 7, No. 11, pp. 653–664, 2010.

20. Taurin, S., H. Nehoff, and K. Greish, "Anticancer Nanomedicine and Tumor Vascular Permeability; Where is the Missing Link?", *Journal of Controlled Release*, Vol. 164, No. 3, pp. 265–275, 2012.

21. Maeda, H., G. Y. Bharate, and J. Daruwalla, "Polymeric Drugs for Efficient Tumor-Targeted Drug Delivery Based on EPR-Effect", *European Journal of Pharmaceutics and Biopharmaceutics*, Vol. 71, No. 3, pp. 409–419, 2009.

22. Raval, N., R. Maheshwari, H, Shukla, K. Kalia, V. P. Torchilin, and R. K. Tekade, "Multifunctional Polymeric Micellar Nanomedicine in the Diagnosis and Treatment of Cancer", *Materials Science and Engineering: C*, Volume 126, p. 112186, 2021.

23. Jain, R. K., “Barriers to Drug-Delivery in Solid Tumors”, *Scientific American*, Vol. 271, No. 1, pp. 58–65, 1994.

24. Fu, X., Y. Shi, T. Qi, S. Qiu, Y. Huang, X. Zhao, X. Sun, and G. Lin, “Precise Design Strategies of Nanomedicine for Improving Cancer Therapeutic Efficacy Using Subcellular Targeting”, *Signal Transduction and Targeted Therapy*, Vol. 5, pp. 262, 2020.

25. Meyer, A., J. Auernheimer, A. Modlinger, and H. Kessler, “Targeting RGD Recognizing Integrins: Drug Development, Biomaterial Research, Tumor Imaging and Targeting”, *Current Pharmaceutical Design*, Vol. 12, No. 22, pp. 2723–2747, 2006.

26. Miura, Y., T. Takenaka, K. Toh, S. Wu, H. Nishihara, M. R. Kano‖, Y. Ino, T. Nomoto, Y. Matsumoto, H. Koyama, H. Cabral, N. Nishiyama, and K. Kataoka, “Cyclic RGD-Linked Polymeric Micelles for Targeted Delivery of Platinum Anticancer Drugs to Glioblastoma through the Blood–Brain Tumor Barrier”, *ACS Nano*, Vol. 7, No. 10, pp. 8583–8592, 2013.

27. Sudimack, J., and R. J. Lee, “Targeted Drug Delivery via the Folate Receptor”, *Advanced Drug Delivery Reviews*, Vol. 41, No. 2, pp. 147–162, 2000.

28. Zhang, Q., X. Wang, P. Z. Li, K. T. Nguyen, X. J. Wang, Z. Luo, H. Zhang, N. S. Tan, and Y. Zhao, “Biocompatible, Uniform, and Redispersible Mesoporous Silica Nanoparticles for Cancer-Targeted Drug Delivery In Vivo”, *Advanced Functional Materials*, Vol. 24, No. 17, pp. 2450–2461, 2013.

29. Pham, S. H., Y. Choi, and J. Choi, “Stimuli-Responsive Nanomaterials for Application in Antitumor Therapy and Drug Delivery”, *Pharmaceutics*, Vol. 12, No. 7, p. 630, 2020.

30. Torchilin, V. P., “Multifunctional, Stimuli-Sensitive Nanoparticulate Systems for Drug Delivery”, *Nature Reviews Drug Discovery*, Vol. 13, No. 11, pp. 813–827, 2014.

31. Cui, T., S. Zhang, and H. Sun, “Co-Delivery of Doxorubicin and pH-Sensitive Curcumin Prodrug by Transferrin-Targeted Nanoparticles for Breast Cancer Treatment”, *Oncology Reports*, Vol. 37, No. 2, pp. 1253–1260, 2017.

32. Long H., W. Tian, S. Jiang , J. Zhao, J. Zhou, Q. He, Z. Tang, W. Shen, and J. Wang, “A Dual Drug Delivery Platform Based on Thermo-Responsive Polymeric Micelle Capped Mesoporous Silica Nanoparticles for Cancer Therapy”, *Microporous and Mesoporous Materials*, Vol. 338, pp. 111943, 2022.

33. Gong, F., N. Yang, X. Wang, Q. Zhao, Q. Chen, Z. Liu, and L. Cheng, “Tumor Microenvironment-Responsive Intelligent Nanoplatforms for Cancer Theranostics”, *Nano Today*, Vol. 32, p. 100851, 2020.

34. Tang, S., Q. Meng, H. Sun, J. Su, Q. Yin, Z. Zhang, H. Yu, L. Chen, W. Gu, and Y. Li, “Dual pH-Sensitive Micelles with Charge-Switch for Controlling Cellular Uptake and Drug Release to Treat Metastatic Breast Cancer”, *Biomaterials*, Vol. 114, pp. 44–53, 2017.

35. Du, J. Z., X. J. Du, C. Q. Mao, and J. Wang, “Tailor-Made Dual pH-Sensitive Polymer–Doxorubicin Nanoparticles for Efficient Anticancer Drug Delivery”, *Journal of the American Chemical Society*, Vol. 133, No. 44, pp. 17560–17563, 2011.

36. Ulbrich, K., T. Etrych, P. Chytil, M. Jelínková and B. Říhová, “Antibody-Targeted Polymer–Doxorubicin Conjugates with pH-Controlled Activation”, *Journal of Drug Targeting*, Vol. 12, No. 8, pp. 477–489, 2004.

37. Wei, X., Q. Luo, L. Sun, X. Li, H. Zhu, P. Guan, M. Wu, K. Luo, and Q. Gong, “Enzyme- and pH-Sensitive Branched Polymer–Doxorubicin Conjugate-Based

Nanoscale Drug Delivery System for Cancer Therapy", *ACS Applied Materials & Interfaces*, Vol. 8, No. 18, pp. 11765–11778, 2016.

38. Xu, X., J. Wu, Y. Liu, M. Yu, L. Zhao, X. Zhu, S. Bhasin, Q. Li, E. Ha, J. Shi, and O. C. Farokhzad, "Ultra-pH-Responsive and Tumor-Penetrating Nanoplatform for Targeted siRNA Delivery with Robust Anti-Cancer Efficacy", *Angewandte Chemie International Edition*, Vol. 55, No. 25, pp. 7091–7094, 2016.

39. Zhai, S., X. Hu, Y. Hu, B. Wu, and D. Xing, "Visible Light-Induced Crosslinking and Physiological Stabilization of Diselenide-Rich Nanoparticles for Redox-Responsive Drug Release and Combination Chemotherapy", *Biomaterials*, Vol. 121, pp. 41–54, 2017.

40. Bader, H., H. Ringsdorf, and B. Schmidt, "Watersoluble Polymers in Medicine", *Die Angewandte Makromolekulare Chemie*, Vol. 123, pp. 457–485, 1984.

41. Shukla, A., S. Tiwari, M.P. Singh, S. Singh, M. K. Singh, and A. Kumar, "A Comprehensive Review on Polymeric Micelles: A Promising Drug Delivery Carrier", *Journal of Analytical and Pharmaceutical Research*, Vol. 10, No. 3, pp. 102–107, 2021.

42. Gaucher, G., M. H. Dufresne, V. P. Sant, N. Kang, D. Maysinger, and J. C. Leroux, "Block Copolymer Micelles: Preparation, Characterization and Application in Drug Delivery", *Journal of Controlled Release*, Vol. 109, No. 1–3, pp. 169–188, 2005.

43. Lin, W. J., L. W. Juang, and C. C. Lin, "Stability and Release Performance of a Series of Pegylated Copolymeric Micelles", *Pharmaceutical Research*, Vol. 20, pp. 668–673, 2003.

44. Burt, H. M., X. Zhang, P. Toleikis, L. Embree, and W. L. Hunter, "Development of Copolymers of Poly(D,L-lactide) and Methoxypolyethylene Glycol as Micellar Carriers of Paclitaxel", *Colloids and Surfaces B: Biointerfaces*, Vol. 16, No. 1–4, pp. 161–171, 1999.

45. Shuai, X., H. Ai, N. Nasongkla, S. Kim, and J. Gao, "Micellar Carriers Based on Block Copolymers of Poly(q-caprolactone) and Poly(ethylene glycol) for Doxorubicin Delivery", *Journal of Controlled Release*, Vol. 98, No. 3, pp. 415–426, 2004.

46. Deshmukh, A. S., P. N. Chauhan, M. N. Noolvi, K. Chaturvedi, K. Ganguly, S. S. Shukla, S. S., M. N. Nadagouda, and T. M. Aminabhavi, "Polymeric Micelles: Basic Research to Clinical Practice", *International Journal of Pharmaceutics*, Vol. 532, No. 1, pp. 249–268, 2017.

47. Thurmond II, K. B., H. Huang, C. G. Clark Jr., T. Kowalewski, and K. L. Wooley, Shell Cross-Linked Polymer Micelles: Stabilized Assemblies with Great Versatility and Potential", *Colloids and Surfaces B: Biointerfaces*, Vol. 16, No. 1–4, pp. 45–54, 1999.

48. Shuai, X., T. Merdan, A. K. Schaper, F. Xi, and T. Kissel, "Core-Cross-Linked Polymeric Micelles as Paclitaxel Carriers", *Bioconjugate Chemistry*, Vol. 15, No. 3, pp. 441–448, 2004.

49. Adams, M. L., A. Lavasanifar, and G. S. Kwon, "Amphiphilic Block Copolymers for Drug Delivery", *Journal of Pharmaceutical Sciences*, Vol. 92, No. 7, pp. 1343–1355, 2003.

50. Otsuka, H., Y. Nagasaki, and K. Kataoka, "PEGylated Nanoparticles for Biological and Pharmaceutical Applications", *Advanced Drug Delivery Reviews*, Vol. 55, No. 3, pp. 403–419, 2003.

51. Kursa, M., G. F. Walker, V. Roessler, M. Ogris, W. Roedl, R. Kircheis, and E. Wagner, "Novel Shielded transferrin–polyethylene glycol–polyethyleneimine/DNA Complexes for Systemic Tumor-Targeted Gene Transfer", *Bioconjugate Chemistry*, Vol. 14, No. 1, pp. 222–231, 2003.

52. Smith, P. P., and S. G. Boyes, “Synthesis of Amphiphilic Block Copolymers via Ring Opening Polymerization and Reversible Addition-Fragmentation Chain Transfer Polymerization”, *Journal of Polymer Science*, Vol. 59, No. 1, pp. 43-58, 2020.

53. Keddie, D. J., “A Guide to the Synthesis of Block Copolymers Using Reversible-Addition Fragmentation Chain Transfer (RAFT) Polymerization”, *Chemical Society Reviews*, Vol. 43, No. 2, pp. 496–505, 2014.

54. Moad, G., E. Rizzardo, and S. H. Thang, “End-Functional Polymers, Thiocarbonylthio Group Removal/Transformation and Reversible Addition-Fragmentation-Chain Transfer (RAFT) polymerization”, *Polymer International*, Vol. 60, No. 1, pp. 9–25, 2011.

55. Willcock, H., and R. K O’Reilly, “End Group Removal and Modification of RAFT Polymers”, *Polymer Chemistry*, Vol. 1, No. 2, pp. 149–157, 2010.

56. Perrier, S., “50th Anniversary Perspective: RAFT Polymerization - A User Guide”, *Macromolecules*, Vol. 50, No. 19, pp. 7433–7447 , 2017

57. Klöppel, G. “Neuroendocrine Neoplasms: Dichotomy, Origin and Classifications”, *Visceral Medicine*, Vol. 33, No. 5, pp. 324–330 , 2017.

58. Sakuma, Y., N. Sata, and A. Lefor, “Pancreas Neuroendocrine Tumors: An Introduction”, *Journal of Pancreas*, No. S(3), pp. 321–327 , 2018.

59. Kulke, M.H., M. H. Shah, A. B. Benson 3rd, E. Bergsland, J. D. Berlin, L. S. Blaszkowsky, L. Emerson, P. F. Engstrom, P. Fanta, T. Giordano, W. S. Goldner, T. R. Halfdanarson, M. J. Heslin, F. Kandeel, P. L. Kunz, B. W. Kuvshinoff 2nd, C. Lieu, J. F. Moley, G. Munene, V. G. Pillarisetty, L. Saltz, J. A. Sosa, J. R. Strosberg, J. N. Vauthey, C. Wolfgang, J. C. Yao, J. Burns, and D. Freedman-Cass, “Neuroendocrine Tumors, Version 1.2015”, *Journal of the National Comprehensive Cancer Network*, Vol. 13, No. 1, pp. 78–108, 2015.

60. Zandee, W. T.; K. Kamp, R.C. van Adrichem, R. A. Feelders, and W. W. de Herder, “Effect of Hormone Secretory Syndromes on Neuroendocrine Tumor Prognosis”, *Endocrine Related Cancer*, Vol. 24, No. 7, pp. R261–R274, 2017.

61. Xu, Z., L. Wang, S. Dai, M. Chen, F. Li, J. Sun, and F. Luo, “Epidemiologic Trends of and Factors Associated With Overall Survival for Patients With Gastroenteropancreatic Neuroendocrine Tumors in the United States”, *JAMA Network Open*, Vol. 4, No. 9, p. e2124750, 2021.

62. Dasari, A., C. Shen, D. Halperin, B. Zhao, S. Zhou, Y. Xu, T. Shih, and J. C. Yao, “Trends in the Incidence, Prevalence, and Survival Outcomes in Patients With Neuroendocrine Tumors in the United States”, *JAMA Oncology*, Vol. 3, No. 10, pp. 1335–1342, 2017.

63. Chauhan, A., Q. Yu, N. Ray, Z. Farooqui, B. Huang, E. B. Durbin, T. Tucker, M. Evers, S. Arnold, and L. B. Anthony, “Global Burden of Neuroendocrine Tumors and Changing Incidence in Kentucky” *Oncotarget*, Vol. 9, No. 27, pp. 19245–19254, 2018.

64. Öberg, K., “Neuroendocrine Tumors: A Historical Overview”, *The Oncologist*, Vol. 21, No. 1, pp. 3-10, 2016.

65. Prakash, L., P. Bhosale, J. Cloyd, M. Kim, N. Parker, J. Yao, A. Dasari, D. Halperin, T. Aloia, J. E. Lee, J. N. Vauthey, J. B. Fleming, and M. H. G. Katz, “Role of Fluorouracil, Doxorubicin, and Streptozocin Therapy in the Preoperative Treatment of Localized Pancreatic Neuroendocrine Tumors”, *Journal of Gastrointestinal Surgery*, Vol. 21, No. 1, pp. 155–163, 2017.

66. Al-Toubah, T., B. Morse, E. Pelle, and J. Strosberg, “Efficacy of FOLFOX in Patients with Aggressive Pancreatic Neuroendocrine Tumors After Prior Capecitabine/Temozolomide”, *Oncologist*, Vol 26, No. 2, pp. 115–119, 2021.

67. Dilz, L. M., T. Denecke, I. G. Steffen, V. Prasad, L. F. von Weikersthal, U. F. Pape, B. Wiedenmann, and M. Pavel, “Streptozocin/5-Fluorouracil Chemotherapy is Associated with Durable Response in Patients with Advanced Pancreatic Neuroendocrine Tumours”, *European Journal of Cancer*, Vol. 51, No. 10, pp. 1253–1262 , 2015.

68. Cloyd, J. M., K. Omichi, T. Mizuno, Y. Kawaguchi, C. D. Tzeng, C. Conrad, Y. S. Chun, T. A. Aloia, M. H. G. Katz, J. E. Lee, D. Halperin, J. Yao, J. N. Vauthey, and A. Dasari, “Preoperative Fluorouracil, Doxorubicin, and Streptozocin for the Treatment of Pancreatic Neuroendocrine Liver Metastases” *Annals Surgical Oncology*, Vol. 25, No. 6, pp. 1709–1715, 2018.

69. Yao, J. C., N. Fazio, S. Singh, R. Buzzoni, C. Carnaghi, E. Wolin, J. Tomasek, M. Raderer, H, Lahner, M. Voi, L. B. Pacaud, N. Rouyrre, C. Sachs, J. W. Valle, G. D. Fave, E. van Cutsem, M. Tesselaar, Y. Shimada, D. Y. Oh, J. Strosberg, M. H. Kulke, and M. E. Pave, “Everolimus for the Treatment of Advanced, Non-Functional Neuroendocrine Tumours of the Lung or Gastrointestinal Tract (RADIANT-4): A Randomised, Placebo-controlled, Phase 3 Study”, *Lancet*, Vol. 387, No. 10022, pp. 968–977, 2016.

70. Chan, J. A., L. Blaszkowsky, K. Stuart, A. X. Zhu, J. Allen, R. Wadlow, D. P. Ryan, J. Meyerhardt, M. Gonzalez, E. Regan, H. Zang, and M. H. Kulke, “A Prospective, Phase 1/2 Study of Everolimus and Temozolomide in Patients with Advanced Pancreatic Neuroendocrine Tumor”, *Cancer*, Vol. 119, No. 17, pp. 3212–3218, 2013.

71. Das, S., T. Al-Toubah, and J. Strosberg, “Chemotherapy in Neuroendocrine Tumors”, *Cancers*, Vol. 13, No. 19, p. 4872, 2021.

72. Kunz, P. L., R. R. Balise, L. Fehrenbacher, M. Pan, A. P. Venook, G. A. Fisher, M. A. Tempero, A. H. Ko, W. M. Korn, J. Hwang, and E. K. Bergsland, “Oxaliplatin-Fluoropyrimidine Chemotherapy Plus Bevacizumab in Advanced Neuroendocrine Tumors: An Analysis of 2 Phase II Trials”, *Pancreas*, Vol. 45, No. 10, pp. 1394–1400, 2016.

73. Xie, H., J. Liu, S. Yadav, X. M. Keutgen, T. J. Hobday, J. R. Strosberg, and T. R. Halfdanarson, “The Role of Perioperative Systemic Therapy in Localized Pancreatic Neuroendocrine Neoplasms”, *Neuroendocrinology*, Vol. 110, No. 3–4, pp. 234–245, 2020.

74. Öberg, K., “Consensus Report on the Use of Somatostatin Analogs for the Management of Neuroendocrine Tumors of the Gastroenteropancreatic System”, *Annals of Oncology*, Vol. 15, No. 6, pp. 966–973, 2004.

75. Gomes-Porras, M., J. Cárdenas-Salas, and C. Álvarez-Escolá, “Somatostatin Analogs in Clinical Practice: a Review” *International Journal of Molecular Sciences*, Vol. 21, No. 5, p. 1682, 2020.

76. Bodei, L., M. S. Kidd, A. Singh, W. A. van der Zwan, S. Severi, I. A. Drozdov, A. Malczewska, R. P. Baum, D. J. Kwekkeboom, G. Paganelli, E. P. Krenning, and I. M. Modlin, “PRRT Neuroendocrine Tumor Response Monitored Using Circulating Transcript Analysis: The NETest”, *European Journal of Nuclear Medicine and Molecular Imaging*, Vol. 47, No. 4, pp. 895–906, 2020.

77. Fazio, N., C. A. Cella, M. Del Re, A. Laffi, M. Rubino, P. Zagami, and F. Spada, “Pharmacodynamics, Clinical Findings and Approval Status of Current and Emerging Tyrosine-Kinase Inhibitors for Pancreatic Neuroendocrine Tumors”, *Expert Opinion on Drug Metabolism & Toxicology*, Vol. 15, No. 12, pp. 993-1004, 2019.

78. Sara, Z., R. Serena, G. Francesco, and B. Giovanna, “mTOR Pathway in Gastroenteropancreatic Neuroendocrine Tumor (GEP-NETs)”, *Frontiers in Endocrinology*, Vol. 11, No. 562505, 2020.

79. de Sousa, M.J., L. Gervaso, M. I. Meneses-Medina, F. Spada, O. Abdel-Rahman, and N. Fazio, “Cyclin-dependent Kinases 4/6 Inhibitors in Neuroendocrine Neoplasms: from Bench to Bedside”, *Current Oncology Reports*, Vol. 24, pp. 715–722, 2022.

80. Jaskula-Sztul, R., W. Xu, G. Chen, A. Harrison, A. Dammalapati, R. Nair, Y. Cheng, S Gong, and Chen, H. “Thailandepsin A-loaded and Octreotide-functionalized Unimolecular Micelles for Targeted Neuroendocrine Cancer Therapy”, *Biomaterials*, Vol. 91, pp. 1–10, 2016.

81. Chen, G., R. Jaskula–Sztul, A. Harrison, A. Dammalapati, W. Xu, Cheng, Y., H. Chen, and S. Gong, “KE108-conjugated Unimolecular Micelles Loaded with a Novel HDAC Inhibitor Thailandepsin-A for Targeted Neuroendocrine Cancer Therapy”, *Biomaterials*, Vol. 97, pp. 22–33, 2016.

82. Surujpaul, P. P., C. Gutiérrez-Wing, B. Ocampo-García, F. de M. Ramírez, C. Arteaga de Murphy, M. Pedraza-López, M. A. Camacho-López, and G. Ferro-Flores, “Gold Nanoparticles Conjugated to [Tyr3]Octreotide Peptide”, *Biophysical Chemistry*, Vol. 138, No. 3, pp. 83–90, 2008.

83. Chen, Q., Z. Li, J. Yu, Q. Xie, H. Lu, Y. Deng, J. Chen, W. Zu, L. Huo, Y. Zhnag, W. Song, J. Lan, J. Cai, Z. Huang, Z. Wang, and H. Zhao, “Novel Gold Nanoparticles Targeting Somatostatin Receptor Subtype Two with Near-infrared Light for Neuroendocrine Tumour Therapy”, *Nano Research*, Vol. 15, pp. 9149–9159, 2022.

84. Si, Y., S. Kim, J. Ou, Y. Lu, P. Ernst, K. Chen, J. Whitt, A. M. Carter, J. M. Markert, J. A. Bibb, H. Chen, L. Zhou, R. Jaskula-Sztul, and X. M. Liu, “Anti-SSTR2 Antibody-Drug Conjugate for Neuroendocrine Tumor Therapy”, *Cancer Gene Therapy*, Vol. 28, pp. 799–812, 2020.

85. Saunders, L. R., A. J. Bankovich, W. C. Anderson, M. A. Aujay, S. Bheddah, K. Black, R. Desai, P. A. Escarpe, J. Hampl, A. Laysang, D. Liu, J. Lopez-Molina, M. Milton, A. Park, M. A. Pysz, H. Shao, B. Slingerland, M. Torgov, S. A. Williams, O. Foord, P. Howard, J. Jassem, A. Badzio, P. Czapiewski, D. H. Harpole, A. Dowlati, P. P. Massion, W. D. Travis, M. C. Pietanza, J. T. Poirier, C. M. Rudin, R. A. Stull, and S. J. Dylla, “A DLL3-targeted Antibody-drug Conjugate Eradicates

High-grade Pulmonary Neuroendocrine Tumor-initiating Cells *in vivo*", *Science Translational Medicine*, Vol. 7, No. 302, p. 302ra136, 2015.

86. Dubey, N., R. Varshney, J. Shukla, A. Ganeshpurkar, P. P. Hazari, G. P. Bandopadhaya, A. K. Mishra, and P. Trivedi, "Synthesis and Evaluation of Biodegradable PCL/PEG Nanoparticles for Neuroendocrine Tumor Targeted Delivery of Somatostatin Analog", *Drug Delivery*, Vol. 19, No. 3, pp. 132–142, 2012.

87. Carollo, A., S. Papi, C. M. Grana, L. Mansi, and M. Chinol, "State of the Art and Recent Developments of Radiopharmaceuticals for Pancreatic Neuroendocrine Tumors Imaging" *Current Radiopharmaceuticals*, Vol. 12, No. 2, pp. 107–125, 2019.

88. Kuzuya, M., S. Kondo, and A. Noguchi, "A New Development of Mechanochemical Solid-state Polymerization of Vinyl Monomers: Prodrug Syntheses and its Detailed Mechanistic Study", *Macromolecules*, Vol. 24, No. 14, pp. 4047–4053, 1991.

89. Lin, P., H. Lee, C. Huang, T. Tai, J. Chen, C. Chen, and Y. Su, "Synergistic Antiproliferative Effect of Ribociclib (LEE011) and 5-Fluorouracil on Human Colorectal Cancer", *Anticancer Research*, Vol. 40, No. 11, pp. 6265–6271, 2020.

90. Aristizabal Prada, E.T., S. Nölting, G. Spoettl, J. Maurer, and C. J. Auernhammer, "The Novel Cyclin-Dependent Kinase 4/6 Inhibitor Ribociclib (LEE011) Alone and in Dual-Targeting Approaches Demonstrates Antitumoral Efficacy in Neuroendocrine Tumors in Vitro", *Neuroendocrinology*, Vol. 106, No. 1, pp. 58–73, 2018.

91. Zheng, Y., H. Wang, H. Tan, X. Cui, S. Yao, J. Zang, L. Zhang, and Z. Zhu, "Evaluation of Lung Cancer and Neuroendocrine Neoplasm in a Single Scan by Targeting Both Somatostatin Receptor and Integrin $\alpha_v\beta_3$", *Clinical Nuclear Medicine*, Vol. 44, No. 9, pp. 687–694, 2019.

92. Clausen, M.M., E. A. Carlsen, C. Christensen, J. Madsen, M. Brandt-Larsen, T. L. Klausen, S. Holm, A. Loft, A. K. Berthelsen, N. Kroman, U. Knigge, and A. Kjaer, "First-in-Human Study of [^{68}Ga]Ga-NODAGAE[c(RGDyK)]$_2$ PET for Integrin $\alpha_v\beta_3$ Imaging in Patients with Breast Cancer and Neuroendocrine Neoplasms: Safety, Dosimetry and Tumor Imaging Ability", *Diagnostics*, Vol. 12, p. 851, 2022.

APPENDIX A : COPYRIGHT NOTICES

This Agreement between Boğaziçi University -- Damla Demirkol ("You") and American Association for Cancer Research ("American Association for Cancer Research") consists of your license details and the terms and conditions provided by American Association for Cancer Research and Copyright Clearance Center.

License Number	5580981309727
License date	Jul 02, 2023
Licensed Content Publisher	American Association for Cancer Research
Licensed Content Publication	Clinical Cancer Research
Licensed Content Title	Therapeutic Nanoparticles for Drug Delivery in Cancer
Licensed Content Author	Cho, Kwangjae; Wang, Xu
Licensed Content Date	Mar 3, 2008
Licensed Content Volume	14
Licensed Content Issue	5

Figure A.1. Copyright notice for Figure 1.4.

AMERICAN ASSOCIATION FOR CANCER RESEARCH LICENSE
TERMS AND CONDITIONS

Jul 11, 2023

This Agreement between Boğaziçi University -- Damla Demirkol ("You") and American Association for Cancer Research ("American Association for Cancer Research") consists of your license details and the terms and conditions provided by American Association for Cancer Research and Copyright Clearance Center.

License Number	5586090593969
License date	Jul 11, 2023
Licensed Content Publisher	American Association for Cancer Research
Licensed Content Publication	Clinical Cancer Research
Licensed Content Title	Phase I and Pharmacokinetic Study of Genexol-PM, a Cremophor-Free, Polymeric Micelle-Formulated Paclitaxel, in Patients with Advanced Malignancies
Licensed Content Author	Kim, Tae-You; Kim, Dong-Wan
Licensed Content Date	Jun 1, 2004
Licensed Content Volume	10
Licensed Content Issue	11

Figure A.2. Copyright notice for Figure 1.5.

Figure A.3. Copyright notice for Figure 1.8.

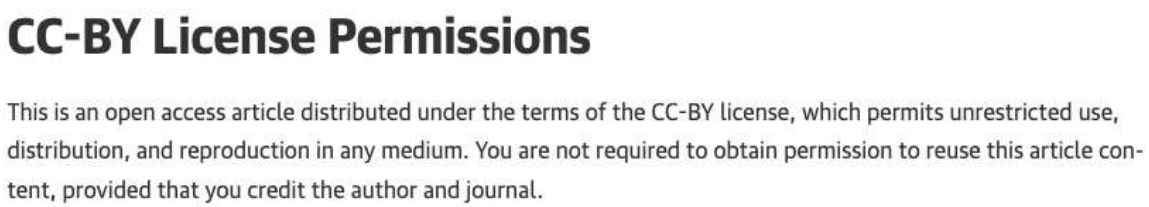

Figure A.4. Copyright notice for Figure 1.11.

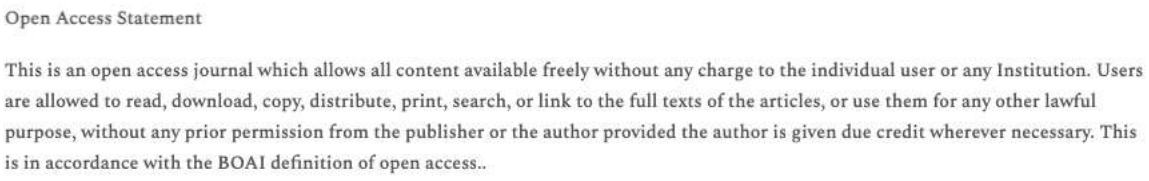

Figure A.5. Copyright notice for Figure 1.12.

This Agreement between Boğaziçi University -- Damla Demirkol ("You") and Elsevier ("Elsevier") consists of your license details and the terms and conditions provided by Elsevier and Copyright Clearance Center.

License Number	5580991064622
License date	Jul 02, 2023
Licensed Content Publisher	Elsevier
Licensed Content Publication	Biomaterials
Licensed Content Title	KE108-conjugated unimolecular micelles loaded with a novel HDAC inhibitor thailandepsin-A for targeted neuroendocrine cancer therapy
Licensed Content Author	Guojun Chen,Renata Jaskula–Sztul,April Harrison,Ajitha Dammalapati,Wenjin Xu,Yiqiang Cheng,Herbert Chen,Shaoqin Gong
Licensed Content Date	Aug 1, 2016
Licensed Content Volume	97
Licensed Content Issue	n/a
Licensed Content Pages	12
Start Page	22
End Page	33

Figure A.6. Copyright notice for Figure 1.13.